

# Assessing the potential of free tropospheric water vapour isotopologue satellite observations for improving the analyses of latent heating convective events

Matthias Schneider<sup>1</sup>, Kinya Toride<sup>2,3,a,b</sup>, Farahnaz Khosrawi<sup>1,c</sup>, Frank Hase<sup>1</sup>, Benjamin Ertl<sup>1,4</sup>, Christopher J. Diekmann<sup>1,d</sup>, and Kei Yoshimura<sup>2,5</sup>

<sup>1</sup>Institute of Meteorology and Climate Research (IMK-ASF), Karlsruhe Institute of Technology, Karlsruhe, Germany

<sup>2</sup>Institute for Industrial Science, The University of Tokyo, Chiba, Japan

<sup>3</sup>Department of Atmospheric Sciences, University of Washington, Seattle, WA, USA

<sup>4</sup>Steinbuch Centre for Computing (SCC), Karlsruhe Institute of Technology, Karlsruhe, Germany

<sup>5</sup>Earth Observation Research Center, Japan Aerospace Exploration Agency, Japan

<sup>a</sup>now at: Cooperative Institute for Research in Environmental Sciences, University of Colorado Boulder, Boulder, Colorado, USA

<sup>b</sup>now at: NOAA Physical Sciences Laboratory, Boulder, Colorado, USA

<sup>c</sup>now at: Forschungszentrum Jülich GmbH, Jülich, Germany

<sup>d</sup>now at: Telespazio Germany GmbH, Darmstadt, Germany

**Correspondence:** M. Schneider  
(matthias.schneider@kit.edu)

**Abstract.** Satellite-based observations of free tropospheric water vapour isotopologue ratios ( $\delta D$ ) with good global and temporal coverage have become recently available. We investigate the potential of these observations for constraining the uncertainties of the atmospheric analyses fields of specific humidity ( $q$ ), temperature ( $T$ ), and  $\delta D$  and of variables that capture important properties of the atmospheric water cycle, namely the vertical velocity ( $\omega$ ), the latent heating rate ( $Q_2$ ), and the precipitation rate (Prcp). Our focus is on the impact of the  $\delta D$  observations ~~if used in addition to the~~ relative to the impact achieved by the observation of  $q$  and  $T$ , which are much easier to be observed by satellites and routinely in use for atmospheric analyses. For our investigations we use an Observing System Simulation Experiment, i.e. simulate the satellite observations of  $q$ ,  $T$ , and  $\delta D$  with known uncertainties ~~, then use them and coverage (e.g. observations are not available for cloudy conditions, i.e. at locations where the atmosphere is vertically unstable).~~ Then we use the simulated observations within a Kalman filter based assimilation framework in order to evaluate their potential for improving the quality of atmospheric analyses. The study is made for low latitudes ( $30^\circ S$  to  $30^\circ N$ ) and for 40 days between mid-July and end of August 2016. We find that ~~the assimilation of  $q$  and  $T$  observations alone well constrains the atmospheric  $q$  and observations have generally the largest impacts on the analyses quality, and that  $T$  fields (analyses skills in the free troposphere of up to 60%), and moderately constrains the fields of observations have overall stronger impacts than  $\delta D$ ,  $\omega$ ,  $Q_2$ , and Prcp (analyses skills of 20%-40%). The additional assimilation of observations. We show that there is no significant impact of  $\delta D$  observations further improves the quality of the analyses of all variables. We use  $Q_2$  as proxy for the presence of condensation and evaporation processes, and we show that the additional improvement is rather weak when evaporation or condensation are negligible (additional analyses skills of~~

generally below 5%), and strongest for high condensation rates (additional skills of about 15% and above)  $\delta D$  observations for stable atmospheric conditions; however, for very unstable conditions the impact of  $\delta D$  observations is significant and even slightly stronger than the respective impact of  $T$  observations. The very high condensation rates (identified by large positive  $Q_2$  values) unstable conditions are rare, but related to extreme events (very high  $\omega$  and  $Prep$ ) that are not well captured in the analyses (for these extreme events also the analyses uncertainties of  $\omega$ ,  $Q_2$ , and  $Prep$  are very large e.g. storm, flooding), i.e. the additional assimilation of  $\delta D$  observations significantly improves the analyses of the water cycle related variables for the events when an improvement is most important. In real world satellite datasets impact on the analyses quality of the events that have the largest societal impact. At the location and time of these unstable atmospheric conditions, no observations are available indicating to a unique remote impact of elsewhere available  $\delta D$  observations on the analyses of convective events. Concerning real world applications, we conclude that the situation of  $\delta D$  observations affected by such strong latent heating events are frequently available, suggesting that the here demonstrated additional satellite observations is very promising, but that further improving the model's linkage between convective processes and the larger scale  $\delta D$  impact for the simulated world is also a realistic scenario for a real world data assimilation fields might be needed for optimising the assimilation impact of real world  $\delta D$  observations.

## 1 Introduction

Clouds and water vapour control atmospheric radiative heating/cooling and condensation or evaporation of water determines where latent heating or latent heat consumption takes place heat is released or consumed. The heating patterns then drive atmospheric circulation, thereby causing whereby in particular vertical transport causes additional evaporation/condensation and impacting on impacts the distribution of water vapour and clouds, which in turn again modify the latent and radiative heating patterns of the atmosphere. This strong coupling between moisture pathways, diabatic heating and atmospheric circulation is responsible for important climate feedback mechanisms (e.g. Sherwood et al., 2014; Bony et al., 2015) and often is is often connected to the evolution of severe weather events (e.g. Fink et al., 2012; Evans et al., 2017). In this context, it is rather worrisome that the diabatic heating rates and the realed vertical transport obtained from different current global reanalyses show significant inconsistencies (e.g. Chan and Nigam, 2009; Ling and Zhang, 2013).

For the generation of daily and global scale analyses, the operational assimilaton systems assimilate the outgoing microwave or infrared radiation (e.g. Eyre et al., 2022). This radiation contains information on the atmospheric state (mostly atmospheric specific humidity,  $q$ , and temperature,  $T$ ). There are many different satellites that measure this spectrally-resolved radiation, including operational weather satellites, like the European Meteosat- and Metop-series (<https://www.eumetsat.int/our-satellites/meteosat-series> and <https://www.eumetsat.int/our-satellites/metop-series>, respectively).

In this study, we investigate the information that free tropospheric  $\delta D$  isotopologue ratio observations can provide in addition to the information provided by the observations of  $q$  and  $T$  for improving the analyses. The ratio is calculated between the heavy isotopologue  $HD^{16}O$  and the main isotopologue  $H_2^{16}O$  in the vapour phase

$$\delta D = \frac{HD^{16}O/H_2^{16}O}{R_{VSMOW}} - 1, \quad (1)$$

where  $\text{H}_2^{16}\text{O}$  and  $\text{HD}^{16}\text{O}$  are the concentrations of the respective isotopologues and  $R_{\text{VSMOW}} = 3.1152 \times 10^{-4}$  is the Vienna Standard Mean Ocean Water ratio of the two isotopologues (this is a standard ratio typically encountered in Ocean water, Craig, 1961). Our particular interest is in  $\delta\text{D}$ , because it is very promising for improving the analysed [vertical transport and](#) latent heating rates: firstly, it can be observed with a reasonable precision by satellite on a daily and almost global scale (e.g. Diekmann et al., 2021a) and secondly, it is ~~affected by condensation/evaporation and thus closely linked to latent heating processes~~ [\(e.g. Galewsky et al., 2016\) strongly affected by vertical transport and convective processes](#) (e.g. Bony et al., 2008; Risi et al., 2008; Noone, 2012).

During the last 15 years, tropospheric  $\delta\text{D}$  products have been developed for different satellite sensors (e.g. Worden et al., 2007; Frankenberg et al., 2009; Schneider and Hase, 2011; Lacour et al., 2012; Boesch et al., 2013; Worden et al., 2019; Schneider et al., 2020). Meanwhile, different weather and climate models have the water isotopologues and the relevant physical processes implemented and can provide modelled isotopologue fields on a global and regional scale at different horizontal resolutions (e.g. Yoshimura et al., 2008; Risi et al., 2010; Werner et al., 2011; Pfahl et al., 2012; Eekstein et al., 2018) [\(e.g. Yoshimura et al., 2008\)](#). This offers advanced opportunities for studying atmospheric moisture processes with water isotopologues.

The tropospheric water vapour isotopologue composition has been used for investigating water cycle related biases in atmospheric models (e.g. Risi et al., 2012; Field et al., 2014; Schneider et al., 2017), ~~clouds and/or precipitation involving processes~~ [processes involving clouds or precipitation](#) (e.g. Webster and Heymsfield, 2003; Worden et al., 2007; Blossey et al., 2010; Field et al., 2010; Bailey et al., 2015; Diekmann et al., 2021b), local diurnal-scale moisture transport (Noone et al., 2011; González et al., 2016), and large-scale moisture transport (e.g. Noone, 2012; González et al., 2016; Lacour et al., 2017; Dahinden et al., 2021).

We use a data assimilation framework together with an OSSE (Observation System Simulation Experiment) to document the added value of the free tropospheric  $\delta\text{D}$  satellite observations, i.e. we simulate satellite observations and then evaluate the theoretical impact of assimilating the observations. This assimilation framework was presented in Yoshimura et al. (2014) and has already been applied by Toride et al. (2021) and Tada et al. (2021). Here we simulate the observations in line with the temporal and horizontal coverage achieved by the IASI (Infrared Atmospheric Sounding Interferometer, Clerbaux et al., 2009) satellite sensor. We simulate the IASI data of  $q$ ,  $T$ , and  $\delta\text{D}$  as generated for the free troposphere by using the retrieval processor MUSICA (MULTi-platform remote Sensing of Isotopologues for investigating the Cycle of Atmospheric water, Schneider et al., 2016, 2022). We evaluate the analyses of the atmospheric fields of  $q$ ,  $T$ ,  $\delta\text{D}$ , the vertical velocity ( $\omega$ ), the latent heating rate ( $Q_2$ ), and the precipitation rate (Prcp). The latter three are strongly coupled and linked to climate feedbacks and weather events. The atmospheric dynamics (expressed among others by  $\omega$ ) is coupled to  $Q_2$ , which in turn affects the vertical thermal structure and thus dynamics. Prcp describes the removal of moisture from the atmosphere, which in turn affects the  $Q_2$  and radiative heating potential.

This study is complementary to Toride et al. (2021), where observations from different platforms and different temporal and spatial coverages were used (satellite, radiosonde and surface observations). The different observational techniques provide diverse information; however, using observations that have a spatial and temporal coverage that differs from the coverage of the IASI  $\delta\text{D}$  data, makes it difficult to understand whether an improvement in the analysis is due to the complementarity of the

information provided by  $\delta D$  or from the complementary coverage (the coverage of IASI  $\delta D$  is much better than the coverage of radiosonde data and more homogeneous than the coverage of the surface data and data from geostationary satellites, see Figs. S4 and S5 in the Supporting Information of Toride et al., 2021). In our OSSE all observations have the same spatial and temporal coverage (the coverage of the MUSICA IASI water isotopologue satellite data, Diekmann et al., 2021a), which assures that any  
90 improvement in the analysis by an additional assimilation of  $\delta D$  is due to the complementarity of the information provided by  $\delta D$  and not affected by different coverages. Furthermore, we investigate the assimilation of  $\delta D$  in addition to the assimilation of satellite observations of  $q$  and  $T$ . The latter (i.e. ~~IASI observations of  $T$  satellite observations~~) were not considered in Toride et al. (2021), despite the fact that they are available with ~~very~~-good quality. Moreover, in addition to the general impact study given by Toride et al. (2021), this work investigates the situations when the isotopologue observations can make a unique  
95 contribution (versus the situations when they have no significant impact).

In Tada et al. (2021) real IASI  $\delta D$  observations (only  $\delta D$  observations) were assimilated and it was shown that such assimilation leads to a better agreement with the ERA5 reanalyses (Hersbach et al., 2020) than not assimilating any data. However, they did not investigate the much larger impact that can already be achieved by assimilating more easily observable data like  $q$  and  $T$ . In this context, our study has a very different focus: we ~~first estimate the impact of assimilating~~ use the assimilation of the  
100 easily observable data ( $q$  and  $T$ ) ~~and then as the reference and~~ evaluate the impact of additionally assimilating  $\delta D$  observations.

The manuscript is structured as follows: section 2 describes the simulated data and the OSSE, the performed assimilation experiments, and the analysed atmospheric variables and the methods used for evaluating their quality. In Sect. 3, we give an overview on the analyses quality improvements achieved by the different assimilation experiments. Section 4 examines ~~in~~  
~~detail the atmospheric events when the additional assimilation of~~ for what atmospheric conditions the  $\delta D$  has observations have  
105 the strongest impact on the analyses and it briefly discusses ~~the possibilities of achieving such impacts also~~ some challenges that have to be overcome for achieving an optimal  $\delta D$  assimilation impact for real world analyses. A summary of the study is given in Sect. 5.

## 2 Data and evaluation

### 2.1 Data simulations

110 We use the isotopologue enabled atmospheric general circulation model IsoGSM (Yoshimura et al., 2008) and simulate the atmospheric state for the two months of July and August 2016, in 6 hour time steps, with a spectral model grid resolution T62 (about 200 km horizontal resolution and 28 vertical sigma levels). We use these simulations as the truth and refer to it in the following as the nature data ( $x_{n_{i,j}}$ , where the index  $i$  indicates the time step and the index  $j$  the location).

For our OSSE we ~~interpolate the  $x_{n_{i,j}}$  data to the locations and time step where satellite observations are available. However,~~  
115 ~~MUSICA IASI data resampled to the IsoGSM grid points are used, which strongly reduces the number of observational data: while there are typically 30 high quality observations each day in a~~ consider that a thermal infrared sensor like IASI offers no free tropospheric trace gas products in the presence of mid- and high-level clouds, so we limit the observational data availability to time steps and locations where the model is free of mid- and high-level clouds. Furthermore, we take into

**Table 1.** Table summarizing the typical free tropospheric observational error ( $\sigma_o$ ) used for the assimilation experiments. The  $\sigma_o$  values are calculated as the root-squares-sum of MUSICA IASI retrieval noise error ( $\sigma_r$ ) and the spatial representativeness error ( $\sigma_s$ , due to resampling the ~~horizontally highly resolved small~~ MUSICA IASI data ~~ground pixels~~ onto the relatively coarse  $200 \times 200$  km IsoGSM grid).

Observation	$\sigma_o$	$\sigma_r$	$\sigma_s$
$q$	0.30 g/kg	0.12 g/kg	0.27 g/kg
$T$	1.2 K	1.0 K	0.7 K
$\delta D$	14‰	10‰	10‰

120 ~~account IASI's high horizontal resolution (ground pixel diameter of about 12 km at nadir), which is much finer than the 200 km~~  
~~horizontal resolution of IsoGSM. Typically there are about 10-20 high quality MUSICA IASI observations each 12 hours in the~~  
~~200 × 200 km area (Diekmann et al., 2021a), in the OSSE used here this number is reduced to typically 1-2, that is represented~~  
~~by IsoGSM (Diekmann et al., 2021a). We simulate MUSICA IASI observations of  $q$ ,  $T$ , and  $\delta D$  in the middle troposphere~~  
~~(at about 550 hPa). ~~The observational error variances and consider the different horizontal representations of model and~~~~  
~~observation when setting up the observational error variance ( $\sigma_o^2$ ) are estimated. For this purpose, we estimate  $\sigma_o^2$  as the sum~~  
125 ~~of a spatial representativeness error variance ( $\sigma_s^2$ ) and a retrieval error variance ( $\sigma_r^2$ ). The  $\sigma_r$  value is the mean error estimated~~  
~~for the MUSICA IASI data within a IsoGSM grid box (it is typically 0.12 g/kg, 1.0 K, and 10‰ for  $q$ ,  $T$ , and  $\delta D$ , respectively,~~  
~~Diekmann et al., 2021a). For the  $\sigma_s$  values we use the standard deviations of the MUSICA IASI data within the IsoGSM grid~~  
~~box, which is generally of a similar order as  $\sigma_r$ . Table 1 gives a summary of the typically assumed observational errors.~~

130 ~~The In addition to the nature data, the data belonging to the different ensemble members are calculated by have to be~~  
~~simulated. This is done with IsoGSM but with initialisations that are slightly different to the initialisation used from different~~  
~~time steps within the same season of the nature run. These initial conditions are considered independent from the nature run~~  
~~(for more details see Toride et al., 2021). We calculate an ensemble with 96 members, ~~i.e. for each time step we make 96~~~~  
~~additional IsoGSM runs (i.e.  $N_{\text{ens}} = 96$ ).~~

## 2.2 Data assimilation with a Kalman filter

135 For the data assimilation we use the Local Ensemble Transform Kalman Filter (LETKF, e.g. Hunt et al., 2007) method as  
developed for its use with water isotopologue data by Yoshimura et al. (2014). The Kalman filter based data assimilation  
technique optimally combines a model forecast with an observation by considering the respective model and observational  
uncertainties (Kalman, 1960). The result is a best estimate of the atmospheric state (the analyses state vector,  $x^a$ ):

$$x^a = x^b + \mathbf{K}(y - \mathbf{H}x^b), \quad (2)$$

140 where  $\mathbf{x}^b$  is the so-called background state (the model forecast),  $\mathbf{y}$  the observation vector, and  $\mathbf{H}$  the observational operator (a matrix operator which maps the model state into the observation space). The matrix operator  $\mathbf{K}$  is the Kalman gain:

$$\begin{aligned}\mathbf{K} &= \mathbf{B}\mathbf{H}^T(\mathbf{H}\mathbf{B}\mathbf{H}^T + \mathbf{R})^{-1} \\ &= (\mathbf{H}^T\mathbf{R}^{-1}\mathbf{H} + \mathbf{B}^{-1})^{-1}\mathbf{H}^T\mathbf{R}^{-1},\end{aligned}\quad (3)$$

where the first and second line are the so-called  $m$ - and  $n$ -forms, respectively (whose equivalence is shown, for instance, in Chapt. 4 of Rodgers, 2000). The matrix  $\mathbf{B}$  is the uncertainty covariance of the background state (it is calculated as the covariance of the different ensemble runs and thus captures the uncertainty of the model forecasts). Its inverse ( $\mathbf{B}^{-1}$ ) is in the following also referred to as the background knowledge information matrix (it is a measure for the knowledge about the atmospheric state including the statistical dependency of different atmospheric state variables). The matrix  $\mathbf{R}$  is the uncertainty covariance of the observational state (it captures the uncertainties of the observations). If we substitute in Eq. (2)  $\mathbf{K}$  by the second line of Eq. (3) and  $\mathbf{y}$  by  $\mathbf{H}\mathbf{x}$  (the observation  $\mathbf{y}$  is the actual atmospheric state  $\mathbf{x}$  mapped to the observational domain) we get:

$$\mathbf{x}^a = \mathbf{x}^b + (\mathbf{H}^T\mathbf{R}^{-1}\mathbf{H} + \mathbf{B}^{-1})^{-1}\mathbf{H}^T\mathbf{R}^{-1}\mathbf{H}(\mathbf{x} - \mathbf{x}^b),\quad (4)$$

which reveals that the Kalman filter weights the impact of the background and the observation on the analyses reciprocally according to their respective uncertainties. More details on the used LETKF settings, like the localization, the covariance inflation or ensemble size choice, are given in Text S2 of the supplement of Toride et al. (2021).

Our assimilation experiments use observations of specific humidity ( $q$ ), atmospheric temperature ( $T$ ) and the isotopologue ratio of water vapour ( $\delta D$ ) at about 550 hPa, which is the pressure level, where the MUSICA IASI products have generally a very good quality (high sensitivity and low uncertainty). An overview on the performed different assimilation experiments is given by Table 2.

### 160 2.3 Evaluation of the analyses quality

In the assimilation step the ensemble members are corrected according to the information provided by the observation. This results in an ensemble of analysed data. For convenience we interpolate the analyses fields to a regular  $2.5^\circ \times 2.5^\circ$  horizontal grid and to 17 vertical pressure levels between 1000 and 10 hPa. We use the mean value of these analysed data (i.e. the ensemble mean values) as representative for the analysis. For a time step  $i$  and a location  $j$  this ensemble mean is

$$165 \quad \bar{x}_{i,j} = \frac{1}{N_{\text{ens}}} \sum_{m=1}^{N_{\text{ens}}} x_{m,i,j},\quad (5)$$

where  $x_{m,i,j}$  is the ensemble member  $m$  at time step  $i$  and location  $j$ . For each location and time step (each event) we calculate the difference of the ensemble mean and the nature data.

$$\Delta_{i,j} = \bar{x}_{i,j} - x_{n,i,j}.\quad (6)$$

This  $\Delta_{i,j}$  captures the uncertainty for the single event corresponding to time step  $i$  and location  $j$ . This is what we want to evaluate.

**Table 2.** Table summarizing the different assimilation experiments used in this study. The column "Assimilated observations" lists the observations used for the experiment, the column "Symbol" shows the symbol used in the following when referring the respective experiment, the column "Corresponding  $\Delta_{i,j}$ " shows the symbol used for the corresponding  $\Delta_{i,j}$  value, calculated according to Eq. (6), and the column "Corresponding RMSD" shows the symbol used for the corresponding RMSD value, calculated according to Eqs. (7).

Assimilated observations	Symbol	Corresponding $\Delta_{i,j}$	Corresponding RMSD
No observations	{}	$\Delta_{i,j}\{\}$	RMSD{}
$q$	{ $q$ }	$\Delta_{i,j}\{q\}$	RMSD{ $q$ }
$T$ and $\delta D$	{ $q, T$ }	$\Delta_{i,j}\{q, T\}$	RMSD{ $q, T$ }
$q$ and $\delta D$	{ $q, \delta D$ }	$\Delta_{i,j}\{q, \delta D\}$	RMSD{ $q, \delta D$ }
$T$ and $\delta D$	<u>{<math>T, \delta D</math>}</u>	<u><math>\Delta_{i,j}\{T, \delta D\}</math></u>	<u>RMSD{<math>T, \delta D</math>}</u>
$q, T$ and $\delta D$	{ $q, T, \delta D$ }	$\Delta_{i,j}\{q, T, \delta D\}$	RMSD{ $q, T, \delta D$ }

**Table 3.** Table with skill values discussed in this study. The column "Description of skill" outlines what assimilation experiments are used for calculating the skills (the evaluated experiment and the reference experiment, with respect to which the evaluation is performed), the column "Symbol" shows the symbol used in the text when referring the respective skill, and the column "Skill calculation" describes how the skill is calculated according to Eq. (8).

<u>Description of skill</u>	<u>Symbol</u>	<u>Skill calculation</u>
<u>{<math>q</math>} wrt {<math>\}</math></u>	<u>{<math>q</math>}</u>	<u><math>\frac{\text{RMSD}\{\} - \text{RMSD}\{q\}}{\text{RMSD}\{\}}</math></u>
<u>{<math>q, T</math>} wrt {<math>\}</math></u>	<u>{<math>q, T</math>}</u>	<u><math>\frac{\text{RMSD}\{\} - \text{RMSD}\{q, T\}}{\text{RMSD}\{\}}</math></u>
<u>{<math>q, T, \delta D</math>} wrt {<math>\}</math></u>	<u>{<math>q, T, \delta D</math>}</u>	<u><math>\frac{\text{RMSD}\{\} - \text{RMSD}\{q, T, \delta D\}}{\text{RMSD}\{\}}</math></u>
<u>{<math>T, \delta D</math>} wrt {<math>q, T, \delta D</math>}, i.e. the <math>q</math> observation impact</u>	<u>{<math>T, \delta D</math>}{<math>q, T, \delta D</math>}</u>	<u><math>\frac{\text{RMSD}\{q, T, \delta D\} - \text{RMSD}\{T, \delta D\}}{\text{RMSD}\{q, T, \delta D\}}</math></u>
<u>{<math>q, \delta D</math>} wrt {<math>q, T, \delta D</math>}, i.e. the <math>T</math> observation impact</u>	<u>{<math>q, \delta D</math>}{<math>q, T, \delta D</math>}</u>	<u><math>\frac{\text{RMSD}\{q, T, \delta D\} - \text{RMSD}\{q, \delta D\}}{\text{RMSD}\{q, T, \delta D\}}</math></u>
<u>{<math>q, T</math>} wrt {<math>q, T, \delta D</math>}, i.e. the <math>\delta D</math> observation impact</u>	<u>{<math>q, T</math>}{<math>q, T, \delta D</math>}</u>	<u><math>\frac{\text{RMSD}\{q, T, \delta D\} - \text{RMSD}\{q, T\}}{\text{RMSD}\{q, T, \delta D\}}</math></u>

We then calculate the root-mean-squares of the  $\Delta_{i,j}$  uncertainties (root-mean-squares-differences, RMSD) for all events belonging to a group of events  $A$ :

$$\text{RMSD} = \sqrt{\frac{\sum_{(i,j) \in A} \Delta_{i,j}^2}{\sum_{(i,j) \in A} 1}}. \quad (7)$$

175 The group of events  $A$  can include all events (sum over all time steps and locations) or only selected events that fulfil certain criteria. The RMSD values is are a statistically robust metric representing the uncertainty of the analyses data for the events that belong to the group of events  $A$ .

From the RMSD values we then ~~determine~~ determine the skill of an assimilation experiment as:

$$\text{Skill} = \frac{\text{RMSD}\{\text{ref}\} - \text{RMSD}\{\text{exp}\}}{\text{RMSD}\{\text{ref}\}}, \quad (8)$$

where  $\text{RMSD}\{\text{exp}\}$  corresponds to the experiment we want to evaluate and  $\text{RMSD}\{\text{ref}\}$  to the reference experiment with respect to which we want ~~do~~ do to do the evaluation. So the skill informs about the relative change of the RMSD value obtained from an assimilation experiment with respect to a reference assimilation experiment, ~~i.e. it documents the relative improvement of the analyses data with respect to a reference.~~ We use ~~this~~ the skill value throughout the paper for evaluating the quality ~~of the analyses obtained by the~~ the different assimilation experiments. ~~Table 3 gives an overview on the different kind of skill values that are discussed~~

We calculate two different types of skill values. For the first type, we use no data assimilation as the reference assimilation experiment. Here positive values document the relative improvement of the analyses when assimilating observations with respect to using no observations. The first three items in Table 3 correspond to the respective skill values used in this study. ~~Table with skill values discussed in this study. The column "Description of skill" outlines what assimilation experiments are used for calculating the skills (the evaluated experiment and the reference experiment, with respect to which the evaluation is performed), the column "Symbol" shows the symbol used in the text when referring the respective skill, and the column "Skill calculation" describes how the skill is calculated according to Eq. (8).~~ ~~Description of skill Symbol Skill calculation~~  $\{q\}$  wrt  $\{q\}$  skill  $\frac{\text{RMSD}\{\}-\text{RMSD}\{q\}}{\text{RMSD}\{\}} \{T\}$  wrt  $\{T\}$  skill  $\frac{\text{RMSD}\{\}-\text{RMSD}\{T\}}{\text{RMSD}\{\}} \{\delta D\}$  wrt  $\{\delta D\}$  skill  $\frac{\text{RMSD}\{\}-\text{RMSD}\{\delta D\}}{\text{RMSD}\{\}} \{q, T\}$  wrt  $\{q, T\}$  skill  $\frac{\text{RMSD}\{\}-\text{RMSD}\{q, T\}}{\text{RMSD}\{\}} \{q, T\}$  wrt  $\{q\}$  skill  $\frac{\text{RMSD}\{q\}-\text{RMSD}\{q, T\}}{\text{RMSD}\{q\}} \{q, \delta D\}$  wrt  $\{q\}$  skill  $\frac{\text{RMSD}\{q\}-\text{RMSD}\{q, \delta D\}}{\text{RMSD}\{q\}} \{q, T, \delta D\}$  wrt  $\{q, T\}$  skill  $\frac{\text{RMSD}\{q, T\}-\text{RMSD}\{q, T, \delta D\}}{\text{RMSD}\{q, T\}} \{q, T, \delta D\}$  wrt  $\{q, T, \delta D\}$  skill  $\frac{\text{RMSD}\{q, T\}-\text{RMSD}\{q, T, \delta D\}}{\text{RMSD}\{q, T\}}$

For this study, we consider the analyses of the variables specific humidity For the second type, we use the assimilation of all observations ( $q$ ), atmospheric temperature ( $T$ ), and water vapour isotopologue ratio ( $\delta D$ ). ~~For these variables we have also observations that are assimilated (see Sect. 2.2). In addition, we evaluate the analyses of variables that describe the water cycle, but we do not assimilate observations of these variables. The analysed atmospheric water cycle variables are vertical velocity ( $\omega$ ), latent heating rate ( $Q_2$ ) and precipitation rate (Prep).~~ together as the reference, and estimate the degradation of the analyses quality (or "loss of skill") by removing one type of observation. By doing so, we can quantitatively compare the impact of the different observation types on the analyses quality. In the following we refer to this skill value as the observation impact, which is the higher negative the stronger the respective observation impact. The respective skill values that are discussed in this study are listed as the three last items in Table 3.

The  $Q_2$  values are calculated according to the budget analysis (Yanai et al., 1973):

$$Q_2 = -L \left( \frac{\partial q}{\partial t} + \mathbf{v} \cdot \nabla q + \omega \frac{\partial q}{\partial p} \right), \quad (9)$$

where  $L$  is the latent heat of net condensation,  $q$  is the specific humidity,  $\mathbf{v}$  is the horizontal wind vector,  $\omega$  is the vertical velocity, and  $p$  is the pressure.

We work with daily mean 6 hourly analyses data (for the 30°S - 30°N region) of July and August 2016. The ensemble simulations are made using 96 different initial conditions. ~~Therefore, the~~ The ensemble mean at the beginning of the simulation



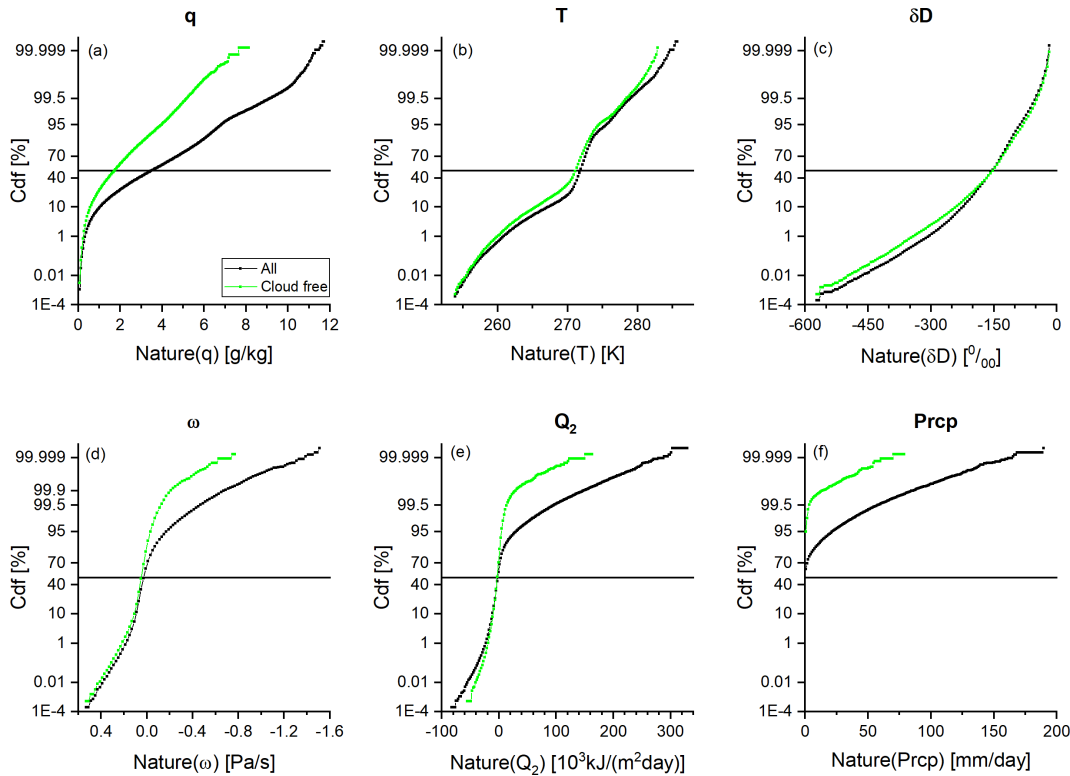


**Figure 1.** Cumulative distribution functions (cdf) of the analysed parameters as obtained from all nature data (black) and from the nature data belonging to cloud-free events (green). (a) For specific humidity ( $q$ ), (b) for temperature ( $T$ ), (c) for the isotopologue ratio ( $\delta D$ ), (d) for vertical velocity ( $\omega$ ), (e) for latent heating ( $Q_2$ ), and (f) for precipitation (Prcp). The 50th percentile is indicated by the black line.

210 period represents climatology. The first three weeks of the simulation (beginning of July) is a "spin-up" period, when the analyses gradually approximate the nature data by assimilating enough observations. In order to avoid impacts of this "spin-up" period, respective data are excluded from the the evaluation study, which is then made for the mid-July to end of August period (covering 4040.75 days).

215 Figure 1 shows the cumulative distribution functions (cdf) of the variables  $q$ ,  $T$ ,  $\delta D$ ,  $\omega$ ,  $Q_2$ , and Prcp, calculated for the evaluated period from the nature data for all time steps and locations (black, full data set) and from the nature data belonging to a location and time step for which we can assimilate observations (green, data subset representing cloud-free conditions only). Only for  $T$  and  $\delta D$ , the full data set and the cloud-free data subset show similar cdfs. Concerning  $q$ ,  $\omega$ ,  $Q_2$ , and Prcp, the respective cdfs are significantly different. For  $q$  all percentiles in the cloud-free data subset are shifted toward drier values if compared to the full data set. For  $\omega$ ,  $Q_2$ , and Prcp, all distributions up to 50th percentiles are comparable for the full data set and the data subset; however, for large percentiles the two cdfs differ significantly. The most extreme values (very low  $\omega$ , very high  $Q_2$  and Prcp) are not present in the cloud-free data subset. This shows that we do not assimilate observations that directly represent the atmosphere of the locations and time steps where these extreme events take place.

220

### 3 Overview on assimilation impacts

This section gives an overview on the assimilation impacts. For this purpose we calculate the RMSD values using all events  
 225 (averaging is performed over all time steps and locations). Equation (7) can then be written as:

$$\text{RMSD} = \sqrt{\frac{1}{N_{\text{loc}}N_{\text{tim}}} \sum_{j=1}^{N_{\text{loc}}} \sum_{i=1}^{N_{\text{tim}}} \Delta_{i,j}^2}, \quad (10)$$

where  $N_{\text{loc}}$  is the number of all locations (here we investigate the 30°S-30°N region with a  $2.5^\circ \times 2.5^\circ$  resolution, i.e.  $N_{\text{loc}} = 3600$ ), and  $N_{\text{tim}}$  is the number of all time steps (here we work with 246 h time steps covering 40.4075 days, i.e.  $N_{\text{tim}} = 40N_{\text{tim}} = 163$ ).

Because for this calculation ~~data of~~, continuous time series are used, we cannot assume independence of the different data  
 230 when estimating the uncertainty of the RMSD values. For this reason, we use the circular block bootstrap method (e.g. Wilks, 2019) for the RMSD uncertainty estimation (the method is also explained in the supplement of Toride et al., 2021). We resample these data 10000 times, which provides a representative distribution of possible RMSD values. Here we use the half of the difference between the respective 15.9th and 84.1th percentile estimates as the  $1\sigma$  uncertainty of the RMSD value, which we then propagate to the skill values.

#### 235 3.1 ~~Standard observations and single type of observations~~ Skill with respect to no data assimilation

Observations of free tropospheric  $q$  and  $T$  contain important information on the atmospheric state (among others on the water cycle variables  $\omega$ ,  $Q_2$ , and Prcp) and are available as standard products from different satellite data processors at global scale, daily coverage, and with good precision. Recently, respective observations of free tropospheric  $\delta D$  have become available.  
 240 ~~which level of analyses quality can be already achieved by assimilating the easily observable variables~~ to what extent these observations help to constrain the model uncertainty.

First we calculate the skills achieved when assimilating  $q$  observations only using no data assimilation as the reference, i.e. here  $\text{RMSD}_{\text{ref}}$  of Eq. (8) is for ensemble means ( $\bar{x}_{i,j}$ ) obtained without assimilating any observation (no data assimilation step). This skill is referred to in the following as the  $\{q\}_{\{\}}$  skill (see Table 3). The ~~light blue~~ black lines in Figure 2a-e show the vertical dependency of the  $\{q\}_{\{\}}$  skills (for Prcp there is naturally no vertical dependency, Fig. 2f). The grey area around the lines indicates the  $1\sigma$  uncertainty of the skills. Because we assimilate the observations of  $q$  at about 550 hPa, highest skill values are generally achieved in the free troposphere around 550 hPa. The dotted lines correspond to the pressure levels at 775 and 350 hPa, which delimits the vertical range we use as representative for the free troposphere and for which we perform dedicated evaluations in Sect.4.

250 In a second experiment we assimilate observations of  $q$  together with  $T$ , which comes very close to an assimilation of relative humidity data. For the evaluation we again calculate the skills with respect to no data assimilation (in the following referred to as the  $\{q, T\}_{\{\}}$  skill, see Table 3). The ~~black~~ magenta lines in Figs. 2a-f give an overview on the achieved  $\{q, T\}_{\{\}}$  skills. Compared to the  $\{q\}_{\{\}}$  skills, these skills are larger in particular for  $T$  around 550 hPa (Fig. 2b), because  $T$  at 550 hPa is

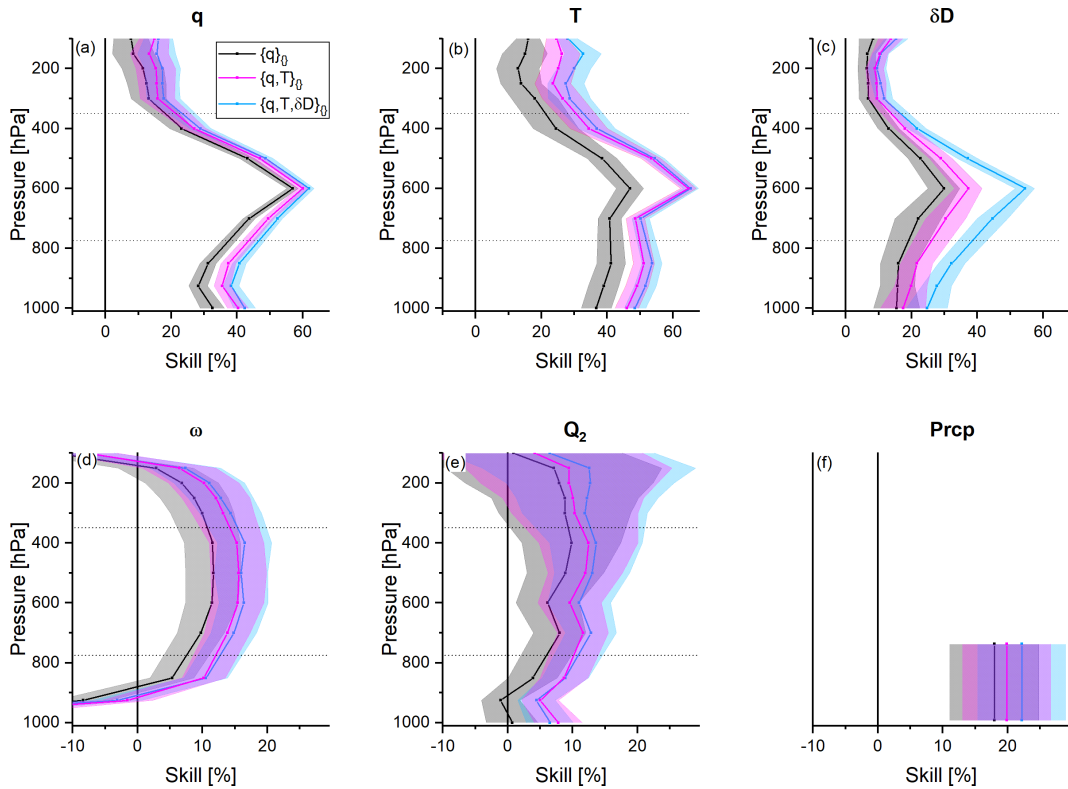


**Figure 2.** Vertical profiles of the skills achieved by assimilating the ~~standard~~ observations (only  ~~$q$  or  $q$  together with and  $T$~~ ) or ~~only one~~ type of observation (only ~~, and  $q$ ,  $T$  or only , and  $\delta D$~~ ) versus assimilating no observations. Light blue:  $\{q\}_T$  skill; Black/grey:  $\{q, T\}_T$   $\{q\}_0$  skill; red/magenta:  $\{T\}_T$   $\{q, T\}_0$  skill; dark yellow/light blue:  $\{\delta D\}_T$   $\{q, T, \delta D\}_0$  skill. The area around the lines represents the  $1\sigma$  uncertainty. (a) For specific humidity ( $q$ ), (b) for temperature ( $T$ ), (c) for the isotopologue ratio ( $\delta D$ ), (d) for vertical velocity ( $\omega$ ), (e) skill for latent heating ( $Q_2$ ), and (f) for precipitation (Prcp).

the additional observation we assimilate. The additional assimilation of  $T$  has also significantly positive impacts on  $q$  and  $Q_2$  above 700 hPa and on  $\delta D$  between 500 and 300 hPa.

By assimilating the standard observations  $q$  and  $T$ , we achieve skills of up to 60% for  $q$  and  $T$  around 600 hPa. Also for the other variables ( $\delta D$ ,  $\omega$ ,  $Q_2$ , and Prcp) – for which no respective observations are assimilated – we get skills that are often between ~~between 30% and 40%~~ 10% and 30%.

In a third and fourth experiment we test the impact when assimilating only  ~~$q$ ,  $T$  or only , and  $\delta D$~~  observations together. For the evaluation we again calculate the skills with respect to no data assimilation (in the following referred to as the  $\{T\}_T$  or  $\{\delta D\}_T$  skills  $\{q, T, \delta D\}_0$  skill, respectively, see Table 3). The red-bright blue lines in Figs. 2a-f give an overview on the achieved  $\{T\}_T$   $\{q, T, \delta D\}_0$  skills. The values are up to 20% for  $q$  (Fig. 2a) and up to 10% for further improved if compared to the  $\{q, T\}_0$  skills: significantly for the  $\delta D$ ,  $\omega$ ,  $Q_2$ , and Prcp (Figs. 2c-f), which is significantly smaller than the  $\{q\}_T$  skill values. Even for  $T$  around 550c, the respective  $\delta D$  skill is above 50% at 600 hPa, the  $\{T\}_T$  skills are only slightly larger

265 than the  $\{q\}_{T}$  skills (Fig. 2 b), i.e. even for the pressure level where the observations are assimilated, but only slightly for the other variables.

### 3.2 Observation impacts of $q$ , $T$ , and $\delta D$

Figure 2 reveals that assimilating  $q$  observations has almost the same positive impact on the  $T$  analyses as assimilating  $T$  observations. For the  $\{\delta D\}_{T}$  skills (dark yellow lines in Figs. 2a-f) the situation is similar. For and  $\delta D$  observations at about 270 550 hPa well constrains the uncertainty of free tropospheric  $q$ ,  $T$ , and  $\delta D$  simulations between about 775 and 350 hPa (skill values up to 60%). There is also a significant improvement for the simulated water cycle variables  $\omega$ ,  $Q_2$  and  $Prep$ , and  $Prp$  (skill values above 20%). In this subsection, we examine the importance of the skills are of a similar order as the  $\{T\}_{T}$  skills and significantly smaller than the  $\{q\}_{T}$  skills (Figs. 2a, d-f). For the different types of observation ( $q$ ,  $T$  analyses the  $\{\delta D\}_{T}$  skills are smaller than the  $\{T\}_{T}$  skills (Fig. 2b) and for the  $T$  and  $\delta D$  analyses it is vice versa (Fig. 2c). For the  $\delta D$  analyses 275 around 550 hPa, the  $\{\delta D\}_{T}$  skill is close to 40%, which is, however, only slightly larger than the respective  $\{q\}_{T}$  skill.

### 3.3 Complementarity of additional observations

The previous subsection reveals that already assimilating the standard observations ( $T$ , respectively) for achieving this analyses quality.

For this purpose we use the experiment that assimilates  $q$  and  $T$  strongly improves the analyses and that the individual impact of  $q$  observations is stronger than the individual impact of  $T$  and  $\delta D$  observations (the latter two have a similar impact). In 280 this subsection, we investigate the complementarity of assimilating  $T$  and  $\delta D$  observations together as the reference, i.e.  $RMSD_{ref}$  of Eq. (8) is for ensemble means ( $\bar{x}_{i,j}$ ) obtained when assimilating observation of  $q$ ,  $T$ , and  $\delta D$  observations on top of  $q$  observations and of assimilating  $\delta D$  observations on top of  $q$  and  $T$  observations together. Then we compare this reference to an experiment for which one observation type has been removed and calculate the respective "loss of skill" values (see 285 last three items of Table 3). A large negative "loss of skill" value means that the respective observation is very important for achieving the analyses quality of the reference experiment, i.e. the respective observation has a strong impact on the analyses quality. Our particular interest is in the complementarity comparing the impact of  $\delta D$  observations, that have become only recently available on global scale and daily coverage. In order to evaluate the complementarity, we calculate the additional skills using the assimilation of the standard observations ( $T$ , to the respective impacts of the traditionally used 290 observations of  $q$  or  $q$  together with and  $T$ ) as the reference, i.e.  $RMSD_{ref}$  of Eq. (8) is for ensemble means ( $\bar{x}_{i,j}$ ) obtained when assimilating observation of  $q$  or when assimilating observations of  $q$  together with  $T$ .

Figure 3a-f shows the same as Fig. 2, but for the additional skills. In order to document the values achieved typically for additional skills, we evaluate these observation impacts. We first evaluate the additional skills for assimilating observations of  $T$  in addition to observations of impact of the  $q$  only, i.e. we calculate the skill of assimilating observations of  $q$  together 295 with observations, which we determine by calculating the loss of skill when assimilating only observations of  $T$  using the assimilation of  $T$  and  $\delta D$  instead of assimilating all three observation types (i.e. the  $q$  observations only as the reference (in the following referred to as the  $\{q, T\}_{T}$  skill observation impact is quantified by the  $\{T, \delta D\}_{\{q, T, \delta D\}}$  skill value, see Table 3). The

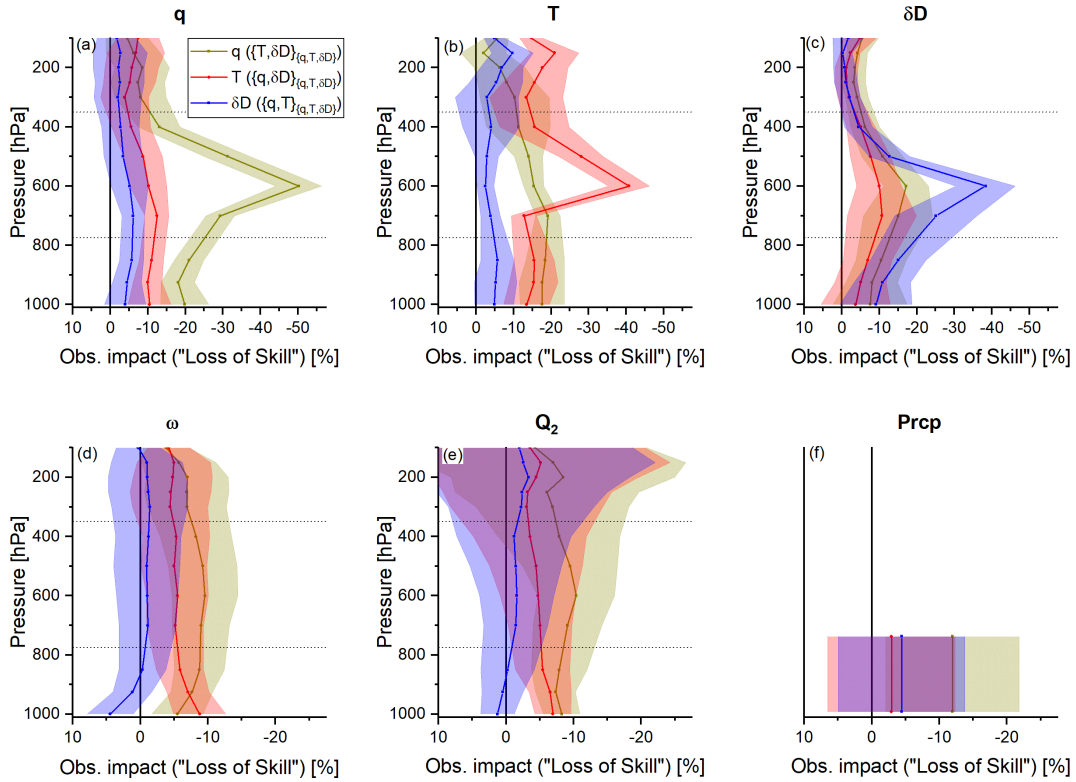


**Figure 3.** Same as Fig. 2, but for the skills achieved by assimilating observations on top Vertical profiles of the standard observations observation impacts ( $q$  and  $T$  "loss of skill" by removing one observation type from the reference experiment that considers all three observation types). Dark yellow: Magenta: impact of  $q$ , represented by the  $\{q, T\}_{\{q, T, \delta D\}}$  skill; olive:  $\{q, \delta D\}_{\{q, T, \delta D\}}$  impact of  $T$ , represented by the  $\{q, \delta D\}_{\{q, T, \delta D\}}$  skill; blue:  $\{q, T, \delta D\}_{\{q, T, \delta D\}}$  impact of  $\delta D$ , represented by the  $\{q, T\}_{\{q, T, \delta D\}}$  skill. The panels (a)-(f) represent the different atmospheric variables as in Fig. 2.

$\{q, T\}_{\{q, T, \delta D\}}$  skills  $q$  observation impacts are represented by the magenta-dark yellow line (and the shaded area is the respective  $1\sigma$  uncertainty of the skill). We observe that, when adding  $T$  as an additional observation, the additional skill is highest for  $T$  and close to 40% removing  $q$  observations, we loose a lot of skill for all atmospheric variables, i.e. the  $q$  observations are important and have a strong impact on all the analysed variables. For the analyses of  $q$  the impact is strongest at 500-600 hPa (loss of skill of up to  $-50\%$ ); for other vertical pressure levels it is smaller, but still the impact is smaller with loss of skill values above or close to  $20-20\%$  (Fig. 3b). Additional observations of  $T$  also improve a). There is also a significant impact of  $q$  observations on the analyses of  $qT$ ,  $\delta D$ ,  $Q_2$ ,  $\omega$  and Prcp (although less than for  $Tq$ ): the  $\{q, T\}_{\{q, T, \delta D\}}$  skills are close to  $15\%$  above 800–20% above 700 hPa for  $qT$  (Fig. 3a) and close to  $10\%$ , close to  $-15\%$  around 600 hPa for  $\delta D$  and  $\omega$  (Figs. 3c+d), above 500 hPa for  $Q_2$  and close to  $-10\%$  for free tropospheric  $\omega$  and  $Q_2$  (Fig. 3e), and d-e) as well as for Prcp (Figs. 3f). By significant, we mean that the calculated loss of skill value is smaller than the estimated  $1\sigma$  uncertainty of the skill, which is represented by the shaded area around the red line.

The ~~green-red~~ line in Fig. 3 represents the ~~additional skills for assimilating observations of  $\delta D$  in addition to observations of  $q$ , i.e. the skill is calculated for assimilating  $T$  observation impact, which we quantify by the "loss of skill" when assimilating only observations of  $q$  and  $\delta D$  observations using the assimilation of  $q$  observations only as the reference (in the following referred to as the  $\{q, \delta D\}_{\{q\}}$  skill instead of assimilating all three observation types (the  $\{q, \delta D\}_{\{q, T, \delta D\}}$  skill value, see Table 3). For  $q$ , we see a significant skill of about 10% for pressure levels above 500 hPa and for The  $T$ , a significant positive skill is only achieved for the 600 observation impact is highest for  $T$ . At 500-600 hPa pressure level the respective loss of skill values are about  $-40\%$  and for other vertical pressure levels they are close to  $-15\%$  (Fig. 3a+b, with significant we mean here that the calculated skill value is larger than the estimated  $1\sigma$  uncertainty of the skill, which is represented by the shaded area around the green line). For b). The  $T$  observations have also a significant impact on the analyses of  $q, \delta D$ , the additional skill is clearly significant and up to 25% around  $Q_2, \omega$  and Prcp (although less than for  $T$ ): the  $\{q, \delta D\}_{\{q, T, \delta D\}}$  skill values are close to  $-10\%$  above 600 hPa, and typically above  $-10\%$  for other the pressure levels above 400 hPa for  $q$  (Fig. 3e), which is reasonable because the additional observation of a) and close to  $-10\%$  at 500-700 hPa for  $\delta D$  is well suited for improving the quality of the  $\delta D$  analyses. For  $\omega$  and  $Q_2$ , the  $\{q, \delta D\}_{\{q\}}$  skills are significant over a large part of the free troposphere, but generally smaller than the respective  $\{q, T\}_{\{q\}}$  skills (Figs (Fig. 3d+e). For Prcp, the  $\{q, \delta D\}_{\{q\}}$  free tropospheric  $\omega$  and  $\{q, T\}_{\{q\}}$  are very similar and close to  $-10\%$  (Fig. 3f) as well as for Prcp the values are still about  $-5\%$  (Figs. 3f)-d-f). However, for Prcp this impact is not significant.~~

In a final ~~assimilation experiment setup~~ we investigate the ~~additional skills for assimilating observations of  $\delta D$  in addition to observations of loss of skills when assimilating only observations of  $q$  and  $T$  instead of all three observation types, i.e. we calculate the  $\{q, T\}_{\{q, T, \delta D\}}$  skill as a measure for the skill is calculated for assimilating  $q, T$ , and  $\delta D$  observations using the assimilation of  $q$  and  $T$  observations as the reference (in the following referred to as the  $\{q, T, \delta D\}_{\{q, T\}}$  skill, observation impact (see Table 3). The overview for the respective additional skills  $\delta D$  observation impact is shown as blue lines in Figs Fig. 3a-f. Concerning the analyses of  $T$ , the additional assimilation of  $\delta D$  observations cannot further improve the analyses quality as already achieved by assimilating observations  $q$  and  $T$ , i.e. the respective  $\{q, T, \delta D\}_{\{q, T\}}$  skills are not significant analyses with respective loss of skill values of close to  $-40\%$  around 600 hPa, and about  $-10$  to  $-30\%$  for other pressure levels above 400 hPa (Fig. 3b). For c), which is reasonable because observation of  $\delta D$  are important for achieving a high quality of the  $\delta D$  analyses. Concerning the  $q$  and  $T$  analyses, the  $\{q, T, \delta D\}_{\{q, T\}}$  are weakly positive and significant between 400 and 800  $\delta D$  observations have a significant impact above 500 hPa (skills are generally below 5%, Fig. 3a for 900-500 hPa the loss of skill values are about  $-5\%$ ). For lower pressure levels the  $\delta D$ , the  $\{q, T, \delta D\}_{\{q, T\}}$  skills are as large as the  $\{q, \delta D\}_{\{q\}}$  skills (up to 25% around 600 hPa observation impact on the  $q$  and  $T$  analyses is not significant (the loss of skill value is smaller than the estimated uncertainty, Fig. 3e), i.e. the  $\delta D$  observations are much more important than the  $T$  observations for improving the analysis quality of  $\delta D$  a+b). For  $\omega$  and  $Q_2$ , there are weak significant the  $\delta D$  observation impact is small and not significant ( $\{q, T\}_{\{q, T, \delta D\}}$  skills of about 5% between 600 and 700 hPa (Fig  $-2.5\%$  only, Figs. 3d+e) and for Prcp, the skill is close the 10% and weakly significant ( For Prcp, we observe a loss of skill value of  $-5\%$ , which suggests that the  $\delta D$  observation impact on the Prcp analyses is slightly stronger than the respective  $T$  observation impact; however, it is not significant (compare red and blue lines in Fig. 3f). This means that~~

~~$\delta D$ -observations provide information on top of  $q$  and  $T$ -observations, that is useful for further improving the quality of the  $\omega$ ,  $Q_2$ , and Prcp analyses.~~

#### 4 The complementarity of $\delta D$ observations

The overview study of the previous section reveals ~~a positive (although weak) impact due to the additional assimilation of that~~ the  $\delta D$  observation impact is overall weak and generally much smaller than the respective impacts of the  $q$  and  $T$  observations. Theoretically the  $\delta D$  data contain unique information on phase transitions, i.e. it might be expected that  $\delta D$  observations can ~~in particularly particular~~ improve the quality of the analyses for atmospheric conditions that involve strong and/or repeated cycles of condensation (or evaporation) processes. In this section we examine the adequacy of this hypothesis in more detail and focus on the analyses of data averaged over a free tropospheric pressure range (775-350 hPa, indicated by the dotted lines in Figs. 2 and 3).

##### 4.1 Analyses quality and ~~atmospheric latent heating~~ vertical velocity

~~If water condenses latent heat is released to the atmosphere and for the evaporation of water energy is needed (heat is removed from the atmosphere, i.e. negative latent heating)~~ For vertically unstable atmospheric conditions repeated cycles of condensation and evaporation take place. For this reason we can ~~use the latent heating rate ( $Q_2$ )~~ examine the aforementioned hypothesis by investigating the dependency of the  $\delta D$  observation impact on atmospheric vertical stability and we use the mass weighted average between 775 and 350 hPa of vertical velocity (free tropospheric  $\omega$ ) as a proxy for ~~phase transitions~~ atmospheric vertical stability.

Figure 4 depicts the dependency of the free tropospheric analyses errors (the  $\Delta_{i,j}$  values, see Eq. (6)) on the free tropospheric ~~latent heating rate ( $Q_2\omega$ )~~ as simulated by the nature run. As in Figs. 2 and 3, we investigate the analyses of the atmospheric variables  $q$ ,  $T$ ,  $\delta D$ ,  $\omega$ ,  $Q_2$ , and Prcp. We examine the low latitudes (30°S - 30°N, with a  $2.5^\circ \times 2.5^\circ$  horizontal resolution) for 40 days with a 6 hourly time resolution, i.e. in total we have ~~144000~~ 586800 events. In order to visualize the distribution of these large amount of data points, we calculate the data densities as follows: we generate 60 equidistant  ~~$Q_2\omega$~~   $Q_2\omega$ -bins covering all occurring  ~~$Q_2\omega$~~   $Q_2\omega$ . Then we calculate the density distribution of the  $\Delta_{i,j}$  values in each  ~~$Q_2\omega$~~   $Q_2\omega$ -bin and sum up the number of data points belonging to the highest  $\Delta_{i,j}$  densities until we consider 98% of all the  $\Delta_{i,j}$  values occurring for the considered  ~~$Q_2\omega$~~   $Q_2\omega$ -bin. These 98% areas are depicted in Fig. 4. The grey filled area represents the  $\Delta\{\}$  distribution (i.e. for the  $\Delta_{i,j}$  values when no observations are assimilated), and the magenta and blue lines the 98% contour lines for the  $\Delta\{q, T\}$  and  $\Delta\{q, T, \delta D\}$  distributions (i.e. for the  $\Delta_{i,j}$  values achieved when we assimilate  $q$  and  $T$  observations and  $q$ ,  $T$  and  $\delta D$  observations, respectively).

Figures 4a-c show the distributions of the  $\Delta_{i,j}$  values for the variables  $q$ ,  $T$ , and  $\delta D$ . There is a weak correlation between the analyses uncertainties and the Nature( $\omega$ ) data, i.e. the  $\Delta(q)_{i,j}$  values tend to be positive for stable atmospheric conditions (positive  $\omega$ ) and negative for unstable atmospheric conditions (strongly negative  $\omega$ ). A weak dependency is also observed in  $\Delta(T)_{i,j}$  and to an even smaller extent in  $\Delta(\delta D)_{i,j}$ : in both cases the largest positive values occur for stable conditions (positive



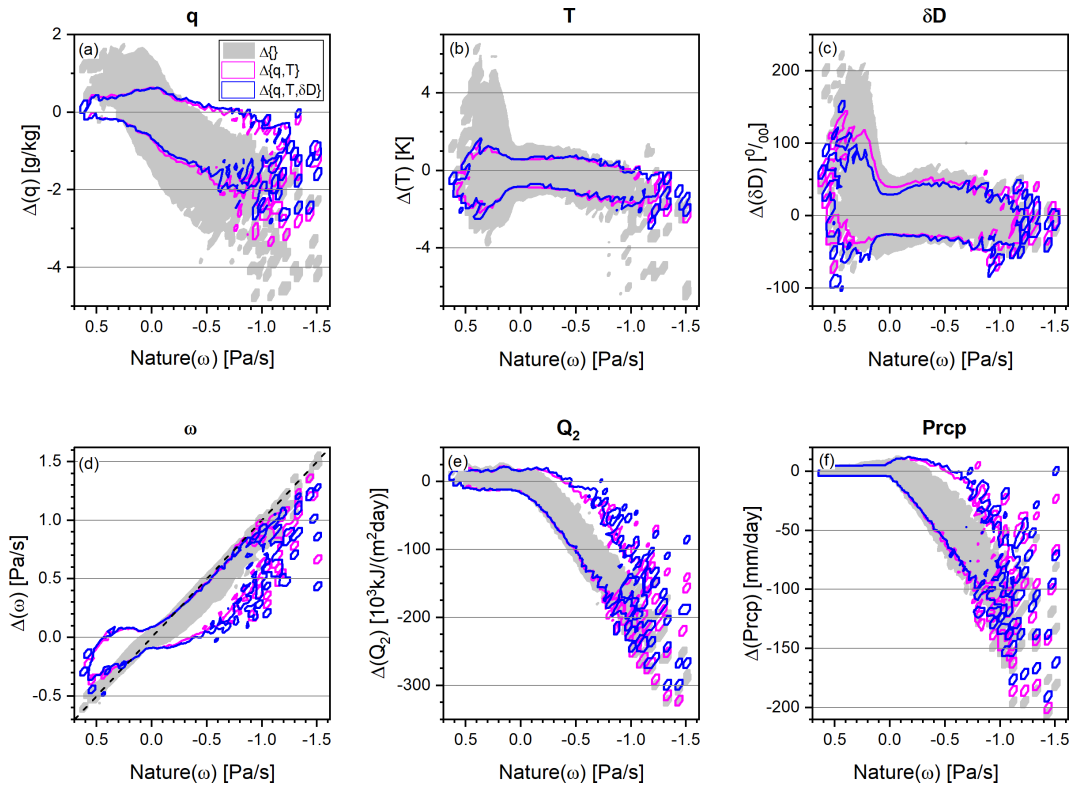


**Figure 4.** Dependency of the free tropospheric analyses errors (mass weighted averages between 775 and 350 hPa) on the free tropospheric heating-rate-vertical velocity (Nature( $Q_2$ ), Nature( $\omega$ )). Shown are the areas that contain 98% of all the  $\Delta_{i,j}$  values for a given Nature( $Q_2$ ), Nature( $\omega$ ) value. Grey: 98% area for no data assimilation (the  $\Delta\{ \}_{i,j}$  data distribution). Magenta line: 98% contour line for the  $\Delta\{q, T\}_{i,j}$  data distribution. Blue line: 98% contour line for the  $\Delta\{q, T, \delta D\}_{i,j}$  data distribution. (a) for specific humidity ( $q$ ), (b) for temperature ( $T$ ), (c) for the isotopologue ratio ( $\delta D$ ), (d) for vertical velocity ( $\omega$ ), (e) skill-for latent heating ( $Q_2$ ), and (f) for precipitation (Prcp, e).

$\omega$  and negative values are more frequent for unstable conditions (negative  $\omega$ ). The assimilation of  $q$  and  $T$  observations approximates the  $\Delta_{i,j}$  values to the respective  $\Delta$ -zero lines. Concerning the  $q$  analyses the additional assimilation of  $\delta D$  observations further reduces the uncertainty in particular for strongly unstable conditions (for highly negative Nature( $\omega$ ) the blue contour line better approximates the  $\Delta$ -zero line than the magenta contour line, Fig. 4a). For  $T$  the additional impact when assimilating  $\delta D$  observation seems also to be slightly larger for unstable conditions (Fig. 4b). For  $\delta D$  the additional impact of assimilating  $\delta D$  observations is most pronounced for stable conditions (blue contour lines better approximates the  $\Delta$ -zero line than the magenta contour for positive  $\omega$  values, Fig. 4c).

When no observations are assimilated, the latent heating-events-strength of atmospheric stability can hardly be identified and the  $Q_2$  uncertainty- $\omega$  error is almost as large as the actual  $Q_2\omega$  value (the  $\Delta\{ \}$  distribution in Fig. 4e-d aligns very closely with the black dashed anti-diagonal-diagonal). The  $\Delta\{q, T\}$  and  $\Delta\{q, T, \delta D\}$  distributions dissipate from the anti-diagonal-diagonal and approximate better the  $\Delta(Q_2)\Delta(\omega)$ -zero line. This reduction of the  $Q_2$ -uncertainty-is-significantly- $\omega$  uncertainty is more



pronounced for the  $\Delta\{q, T, \delta D\}$  than for the  $\Delta\{q, T\}$  distributions, and largest for high actual  $Q_2\omega$  values. However, despite the significant correction, the uncertainty is still largest for the highest  $Q_2\omega$  values. This means that, although the events of strong latent heating vertically unstable atmospheric conditions can be much better identified by assimilating the observations, the absolute strength of the heating instability is still underestimated.

For the analyses of vertical velocity ( $\omega$ ) latent heating ( $Q_2$ , Fig. 4de) and precipitation rate (Prcp, Fig. 4f), the results are very similar to those of  $Q_2\omega$ : without assimilating any data ( $\Delta\{\}$  densities), the analyses are very uncertain for high heating rates (distribution of  $\Delta_{i,j}$  values is far away from the respective  $\Delta$ -zero lines). Actually vertical velocity, precipitation rate, and heating rate are strongly correlated, which means that the events with strong upward motion of air latent heating and/or with high precipitation rates are almost not identified. By assimilating  $q$  and  $T$  observations, this/these uncertainties can be strongly reduced. A further significant reduction (in particular for events when the uncertainty is very high) can be achieved by assimilating  $\delta D$  observations in addition to the observations of  $q$  and  $T$ .

~~Figures 4 a-c show the distributions of the  $\Delta_{i,j}$  values for the variables-~~

## 4.2 The unique $\delta D$ assimilation impact

~~Figure 4 suggests that when assimilating  $q$ , and  $T$ , and together with  $\delta D$ . There are only weak correlations between the analyses uncertainties and the Nature( $Q_2$ ) data. Although the  $\Delta(q)_{i,j}$  values tend to be positive for negative heating rates and negative for positive heating rates, this dependency is much weaker as what is observed for  $\omega$ ,  $Q_2$ , and Prcp. A rather weak dependency is also observed in  $\Delta(T)_{i,j}$  and to an even smaller extent in  $\Delta(\delta D)_{i,j}$ : in both cases the largest positive or negative values occur for negative  $Q_2$ . The assimilation of we get smaller analyses uncertainties for unstable atmospheric conditions than when only assimilating  $q$  and  $T$  observations approximates the  $\Delta_{i,j}$  values to the respective  $\Delta$ -zero lines. Concerning the  $q$  analyses the additional assimilation of  $\delta D$  observations further reduced the uncertainty in particular for events with high latent heating rates (for high Nature( $Q_2$ ) the blue contour line better approximates the  $\Delta$ -zero line than the magenta contour line, Fig. 4a). For  $T$  the additional impact when assimilating  $\delta D$  observation seems also to be slightly larger for high positive or negative heating rates (Fig. 4b). For  $\delta D$  an the additional impact of assimilating  $\delta D$  observations seems to be largely independent on the heating rates (blue contour lines better approximates the  $\Delta$ -zero line than the magenta contour for all  $Q_2$  values, Fig. 4c).~~

## 4.3 The unique $\delta D$ assimilation impact

~~In order to better quantitatively document the dependency between the latent heating rate and the additional impact of assimilating  $\delta D$  observations, we investigate in this subsection how the skills. In this subsection we quantify how the observation impacts depend on the  $Q_2$  nature data atmospheric vertical stability.~~

Figure ~~??~~ 5 shows the abundances of events corresponding to 13 different  $Q_2$  heating rate free tropospheric vertical velocity ( $\omega$ ) bins. We have the highest abundances for heating rates  $\omega$  values that are close to zero. The three bins corresponding to Nature( $Q_2\omega$ ) values between  $-8.3$  and  $+6.5 \times 10^3$   $-0.09$  and  $+0.06$  kJPa/(m<sup>2</sup>day) comprise together 108282 s comprise together 441253 events, which is  $\frac{108282}{144000} = 75.20$   $\frac{441253}{586800} = 75.20\%$  of all events. Extreme heating rates vertical instabilities

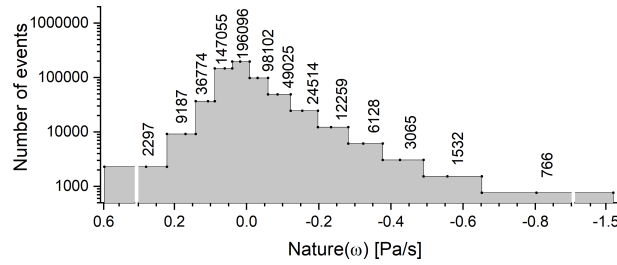


**Figure 5.** Abundance chart showing the number of events for each of the 13  $Q_2\omega$ -bins used for classifying different latent heating strengths atmospheric vertical stability conditions.

420 are rare, e.g. the bin-bins corresponding to Nature( $Q_2$ ) values between  $+110.5$  and  $+262.5 \times 10^3 \omega$  values smaller than  $-0.38 \text{ kPa}/(\text{m}^2 \text{ day})$  only comprises 188 events, i.e. only  $\frac{188}{144000} = 0.13\%$  of all the data points. However, these extreme events are responsible for almost all the intense precipitation events, and it is very important to improve the analyses in a way that allows a better identification of these extreme events.

We use the binning from Fig. ??-5 for evaluating the skill dependence on  $Q_2$ . Therefore, we calculate the dependence of the observation impacts on  $\omega$ . As in Sect. 3, we quantify the observation impacts by the loss of skill values according to the last three items in Table 3. We calculate the respective RMSD values according to Eq. (7) for 13 different groups of events  $A$ . Each of the groups comprises the events showing heating rates-free tropospheric  $\omega$  values as defined by the 13 different bins of Fig. ??. Then for each of the bins we calculate the skill according to Eq. (8)-5. Because the events with high  $Q_2$  values strongly negative  $\omega$  values (convective events) are generally individual events occurring on a single day, the respective groups of events do not consist of continuous time series. For the error estimation, we thus assume that the events of a certain  $Q_2\omega$  group are independent (in the circular block bootstrap method the block size is reduced to only one event).

Figure ?? depicts the skills 6 depicts the observation impacts obtained for the 13 Nature( $Q_2\omega$ )-bins. The colours are as in Fig. 3. Concerning the additional skill for assimilating  $T$  observations on top of The  $q$  observations ( $\{q, T\}_{\{q\}}$  skill observation impact (quantified by the  $\{T, \delta D\}_{\{q, T, \delta D\}}$  skill value, represented by magenta colour), we cannot identify a clear dependency on the  $Q_2$  values. The skills are more or less the same the dark yellow lines) is strong for all analysed variables (as already shown in Fig. 3). The highest  $q$  observation impact is found for  $q$  analyses at stable atmospheric conditions (loss of skill value of about  $-60\%$  for the  $775$  to  $350$  Nature( $\omega$ )  $> +0.1$  hPa-altitude range (overview examination of all events together): highest skills of between  $20\%$  and  $30\%$  are observed for  $T$  (Fig. ??b), skills between  $10\%$  and  $15\%$  are seen for  $q$  (Pa/s, Fig. ??a), and for 6a). For the  $T$  and  $\delta D$  analyses the  $q$  observation impact is strongest, and for the analyses of  $\omega$ ,  $Q_2$ , and Prcpt the skills are generally below  $10\%$ , it is weakest for Nature( $\omega$ ) close to zero (Fig. ??e-f).

The  $\{q, \delta D\}_{\{q\}}$  skills (additional skills for assimilating  $\delta D$  observations on top of 6b+c and Fig. 6d-f, respectively). In summary, there is no clear systematic dependency of the  $q$  observations, represented by olive colour) show a clear dependency on the  $Q_2$  values. For  $q$ , observation impact on atmospheric vertical stability.

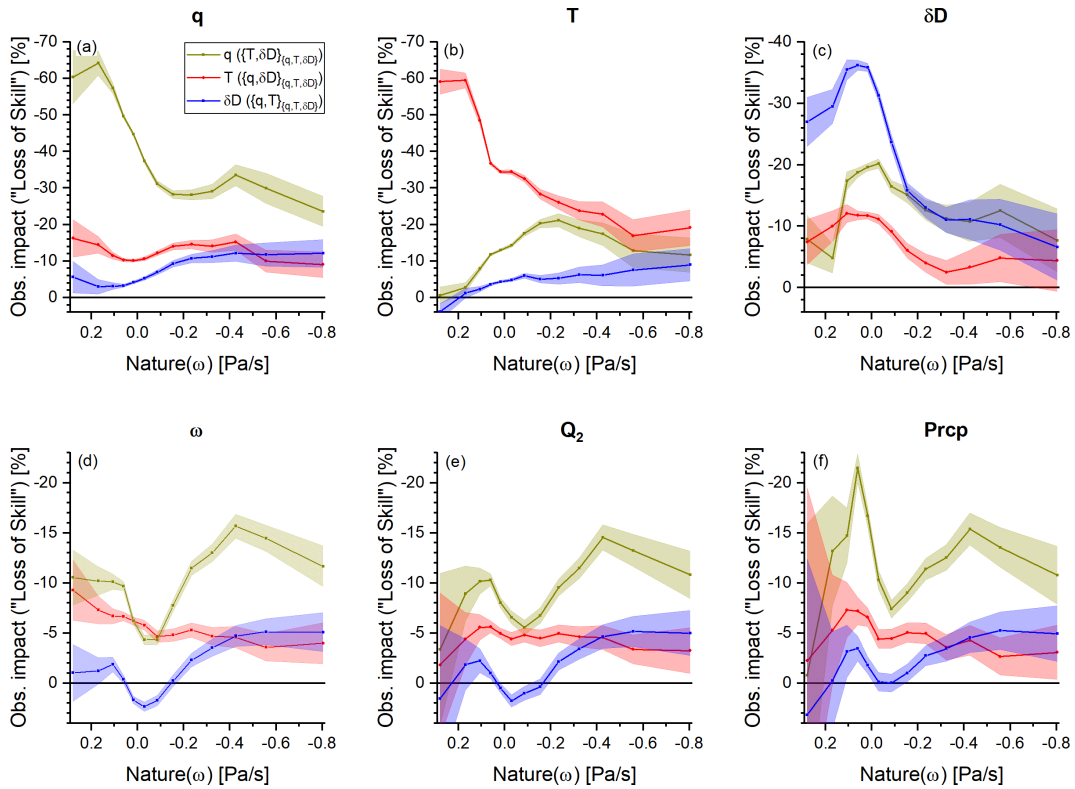


**Figure 6.** Dependency of the skills-free tropospheric observation impacts (mass weighted averages between 775 and 350 hPa) on the free tropospheric latent heating rate-vertical velocity ( $\text{Nature}(Q_2)\text{Nature}(\omega)$ ). The skills are calculated for colours (dark yellow, red, and blue) and the  $Q_2$ -bins panels (a-f) are as depicted in Fig. ??. Shown are the skills achieved by assimilation observations on top of the standard observations<sup>3</sup>: Magenta: they represent the  $\{q, T\}_{(q, T)}$  skill; olive:  $\{q, \delta D\}_{(q, T, \delta D)}$  skill; blue:  $\{q, T, \delta D\}_{(q, T, \delta D)}$  skill. The areas around the lines indicate the  $1\sigma$  uncertainties of the skills. (a) For specific humidity ( $q$ ), (b) for temperature ( $T$ ), (c) for the isotopologue ratio ( $\delta D$ ), (d) for vertical velocity ( $\omega$ ), (e) for latent heating ( $Q_2$ ), different observation impacts and (f) for precipitation (Prep) different analysed atmospheric variables, respectively.

The red lines represent the  $T$ ,  $\omega$ ,  $Q_2$ , and Prep (Figs. ??a,b,d-f) and for low heating rates ( $\text{Nature}(Q_2)$  between  $-15.5$  and  $+36.0 \times 10^3$  observation impact (quantified by the  $\{q, \delta D\}_{(q, T, \delta D)}$  skill value). It is strongest for the  $T$  analyses at stable atmospheric conditions (loss of skill value of about  $-60\%$  for  $\text{Nature}(\omega) > +0.1 \text{ kJPa}/(\text{m}^2 \text{ day})$ ), these skills are smaller than the respective  $\{q, T\}_{(q, T)}$  skills. The respective  $Q_2$  bins comprise 97% of all examined events, which explains that this finding is similar to the one from the overview plot (s. Fig. 3), except for Prep where in the overview plot there is no clear difference between the  $\{q, \delta D\}_{(q, T, \delta D)}$  and  $\{q, T\}_{(q, T)}$  skills. However, for the rare occasions of high heating rates (negative or positive,  $Q_2$  below  $-20 \times 10^3 \text{ kJ}/(\text{m}^2 \text{ day})$  or above  $+70 \times 10^3 \text{ kJ}/(\text{m}^2 \text{ day})$ ) the  $\{q, \delta D\}_{(q, T, \delta D)}$  skills get as large or even larger than (6b). Concerning the analyses of the other atmospheric variables, the  $\{q, T\}_{(q, T)}$  skills. For  $T$  observation impact shows generally a

weak decrease with decreasing  $\text{Nature}(\omega)$ , i.e. the impact tends to be slightly stronger for stable than unstable atmospheric conditions (Figs. 6a,c-f).

455 The  $\{q, T, \delta D\}_{\{q, T, \delta D\}}$  skill values quantify the  $\delta D$  (Fig. ??c) the  $\{q, \delta D\}_{\{q, T\}}$  skills are for all  $Q_2$  values larger than the  $\{q, T\}_{\{q, T\}}$  skills, naturally because the assimilation of  $\delta D$  observations is most important for improving observation impact and they are depicted as blue line in Fig. 6. The strongest  $\delta D$  observation impact is found for the  $\delta D$  analyses for stable atmospheric conditions (for  $\text{Nature}(\omega) > -0.05$  Pa/s the respective loss of skill value is beyond  $-25\%$ , Fig. 6c).

460 The  $\{q, T, \delta D\}_{\{q, T\}}$  skills (additional skills for assimilating  $\delta D$  observations on top of  $q$  and  $T$  observations, represented by blue colour) show a clear dependency on the  $Q_2$  values. For the analyses of all the other variables, the skills are highest for strongly positive or strongly negative  $\text{Nature}(Q_2)$  values. For  $\text{Nature}(Q_2)$  close to zero, the skills are very small (often below 5%, except for  $\delta D$  where it is never below 20%). Because  $\delta D$  observation impact tends to be stronger for unstable if compared to stable atmospheric conditions (Fig. 6a,b,d-f), thus showing the opposite behaviour as the  $T$  observation impact. While for relatively stable atmospheric conditions ( $\text{Nature}(\omega) > -0.2$  Pa/s), the  $T$  observation impact is significantly stronger than the  $\delta D$  observation impact, for unstable conditions ( $\text{Nature}(\omega) < -0.4$  Pa/s), the  $\delta D$  observation impact becomes as strong as the  $T$  observation impact or even slightly exceeds it. Because the large majority of events the heating rates are close to zero (see discussion above correspond to relatively stable atmospheric conditions ( $\text{Nature}(\omega) > -0.2$  Pa/s), the overview study reveals generally small  $\{q, T, \delta D\}_{\{q, T\}}$  skill values as shown in Fig. 3 reveals an overall weak  $\delta D$  observation impact. However,  $\delta D$  observations become very important for for the infrequently occurring events corresponding to extreme heating rates. Then assimilating the unstable atmospheric conditions,  $\delta D$  observations on top of  $q$  and become at least as important as  $T$  observations can strongly improve the quality of the analyses of all variables (skills of 15% and above). This is in particular important for the analyses of  $\omega$ ,  $Q_2$ , and Prcp, because these variables are relatively poorly constrained by the  $q$  and  $T$  observations. The the most extreme  $\omega$ ,  $Q_2$ , and Prcp values are relatively poorly identified by assimilating only  $q$  and  $T$  observations; a better identification of these events is achieved by the additional assimilating assimilation of  $\delta D$  (compare the magenta and blue contour lines in Fig. 4d-f).

### 475 4.3 Discussion and outlook

Different  $\{q, \delta D\}$  pair distributions as seen in the data from the nature run. Shown are the areas that contain 80% of all the data. Dark grey: 80% area when considering all data. Green line: 80% contour line when considering data with  $\text{Nature}(Q_2) < -10 \times 10^3$  kJ/(m<sup>2</sup> day). Blue line: 80% contour line when considering data with  $\text{Nature}(Q_2) > -1 \times 10^3$  kJ/(m<sup>2</sup> day) and  $\text{Nature}(Q_2) < +1 \times 10^3$  kJ/(m<sup>2</sup> day). Red line: 80% contour line when considering data with  $\text{Nature}(Q_2) > +10 \times 10^3$  kJ/(m<sup>2</sup> day). The dotted grey line is a typical tropical Rayleigh line, assuming the following atmospheric condition over the ocean source location:  $T = 25^\circ\text{C}$ ,  $\text{RH} = 80\%$ , and  $\delta D = -80$ . The Moreover, the relatively strong  $\delta D$  observation impact occurs for conditions when there are no observations assimilated: a thermal infrared sensor like IASI offers no free tropospheric products for mid- or high-level clouds, which are typically present for  $\text{Nature}(\omega) < -0.4$  Pa/s (see Fig. 1d). This suggests that the distinct free tropospheric  $\delta D$  signals caused by atmospheric convection (e.g. Risi et al., 2008; Diekmann et al., 2021b) are well conserved in the  $\delta D$  fields modelled for cloud-free locations outside of the convective area. At the cloud-free location the observations can then be exploited by the

assimilation system and allow for improving the analyses of the convective area. The  $\delta D$  observations seems to have a unique remote impact on the analyses of convective regions.

### 4.3 Simulations versus real world data

In order to link our OSSE study to the real world, we examine similarities and differences of the  $\{q, \delta D\}$ -pair distributions between the simulated data used in this study and actual MUSICA IASI observational data. The  $\{q, \delta D\}$ -pair distributions can give valuable insight into the dominating atmospheric processes (mixing, shallow cloud formation and rain-out, convection and extreme precipitation events, Noone, 2012). Figure 7 shows ~~different  $\{q, \delta D\}$ -pair distributions as obtained from the nature simulation run~~ these distributions for different data (sub-)sets. Shown are the areas where the  $\{q, \delta D\}$ -pairs have the highest densities and sum up to ~~80%–90% (thick contour lines) and 50% (thin contour lines)~~ of all the available data. The distributions are determined for all 144000 events and for three different subsets of events belonging to three different latent heating categories: data.

~~The dark grey area comprises the area where 80% of all the 144000 data points are located~~ Concerning the OSSE data, the black lines show the distribution for the full nature run data set (586800 events for the studied 40 days and the 30°S–30°N area). The thick grey dotted line represents a typical tropical Rayleigh line (starting conditions:  $T = 25^\circ\text{C}$ ,  $\text{RH} = 80\%$ , and  $\delta D = -80\%e_s$ ). We observe that ~~for most of the events the~~ the  $\{q, \delta D\}$ -pairs are located above well distributed around the Rayleigh line, ~~indicating that mixing processes very importantly affect the nature simulations (Noone et al., 2011; González et al., 2016)~~

~~The green contour line comprises 80% of all the events with strongly negative latent heating rates (Nature( $Q_2$ ) below  $-10 \times 10^3 \text{ kJ}/(\text{m}^2\text{day})$ ).~~ These subset of events is more affected by mixing between dry/depleted and humid/enriched water masses than the average of all events (indicated by a  $\{q, \delta D\}$ -pair distribution moving to lower  $q$ , but higher  $\delta D$  values). For the subset that comprises the events where  $Q_2$  is negligible (within  $\pm 1 \times 10^3 \text{ kJ}/(\text{m}^2\text{day})$ , blue contour line), mixing between dry/depleted and ~~For dry conditions, the data points tend to lie above the Rayleigh line, which indicates that the respective humidity levels are largely controlled by mixing between humid/enriched end-members is also important, but in difference to the green contour lines, here we have a significant number of  $\{q, \delta D\}$ -pairs with very low  $q$  and low  $\delta D$ . This strong depletion together with low humidity suggest that the and dry/depleted end-member is dominating the mixed water mass. We found that this is correlated to the events with the highest positive vertical velocity values, i.e. strong downwelling of upper tropospheric air into the middle troposphere. This typically happens in the subtropics and makes the free tropospheric air very dry (very low relative humidities), i.e. neither condensation nor evaporation is happening, and there is no latent heating.~~

~~The red contour line comprises the events with strongly positive latent heating rates (Nature( $Q_2$ ) above  $+30 \times 10^3 \text{ kJ}/(\text{m}^2\text{day})$ ).~~ The  $\{q, \delta D\}$ -pair corresponding to these events are generally located water masses (Noone et al., 2011; González et al., 2016). For humid conditions, the data points tend to be situated below the Rayleigh line, i.e. in the super-Rayleigh domain (Noone, 2012). This strong depletion together with high humidity is caused by recurring evaporation and condensation, i.e. the same water mass experiences several condensation/evaporation processes in the atmosphere. This is a typical free tropospheric  $\{q, \delta D\}$ -

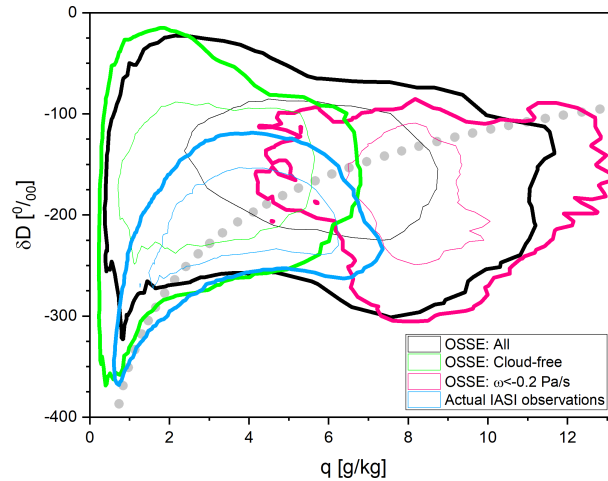


**Figure 7.** Distributions of  $\{q, \delta D\}$ -pairs at about 600 hPa as derived from the different data sets. Shown are the contour lines for the highest  $\{q, \delta D\}$ -pair data density (thick and thin lines show the areas containing 90% and 50% of all the data, respectively). Black: all data from the nature run; green line: cloud-free data from the nature run, i.e. data used as observations during the assimilation step; pink: nature run data corresponding to unstable atmospheric conditions ( $\text{Nature}(\omega) < -0.2 \text{ Pa/s}$ ). Bright blue: actual IASI observation data. The dotted grey line is a typical tropical Rayleigh line, assuming the following atmospheric condition over the ocean source location:  $T = 25^\circ\text{C}$ ,  $\text{RH} = 80\%$ , and  $\delta D = -80\text{‰}$ .

pair signal for convective activity (e.g. Blossey et al., 2010; Diekmann et al., 2021b). According to (e.g. Risi et al., 2008; Blossey et al., 20

520

The green contour lines represent the distribution for the atmospheric conditions, for which observations are assimilated in our assimilation studies. These are the cloud-free and stable atmospheric conditions. For this data subset, the  $\{q, \delta D\}$ -pairs are mostly located below  $q = 6 \text{ g/kg}$  and above the Rayleigh line, caused by the aforementioned dry air mass mixing.

The pink contour line comprises the events corresponding to unstable atmospheric conditions ( $\text{Nature}(\omega) < -0.2 \text{ Pa/s}$ ). The respective  $\{q, \delta D\}$ -pairs are generally located in the aforementioned super-Rayleigh domain, which suggests convective activity. From Figs. 4 and ??, it is 6 we can conclude that the  $\delta D$  observations made in have the strongest impact on the analyses of the events with  $\text{Nature}(\omega) < -0.2 \text{ Pa/s}$ , i.e. for events where the  $\{q, \delta D\}$ -pairs show this super-Rayleigh domain, that most importantly improve the analyses. distribution. However, this is very different from the distribution of the assimilated data (green contour lines), revealing again that we do not assimilate observation of convective atmospheres (recall the discussion in the context of Fig. 1).

530

These findings enable us to give some outlook on the possibility of improving real-world analyses with real-world

The  $\{q, \delta D\}$ -pair satellite data, similarly to the improvements as demonstrated here theoretically with our OSSE. In the MUSICA IASI distribution obtained from actual MUSICA IASI observations is represented by the bright blue contour lines in Fig. 7 for the same period and locations as the OSSE data. This real world data are only available for a cloud-free atmosphere.

Obviously, there is a significant difference between the  $\{q, \delta D\}$ -pair satellite data super-Rayleigh conditions are often observed.

535

~~They are, for instance, reported for the central Pacific distribution simulated for cloud-free conditions and the actually observed distributions (compare green and bright blue contour lines in Fig. 11 of Schneider et al. (2017) or for West Africa in Fig. 14 of Diekmann et al. (2021a) and in Chapt. 7). Whereas the  $q$  values in the simulations and the real world observations are very similar, the respective  $\delta D$  values are systematically by about 50-100‰ lower in the observations if compared to the simulations~~  
540 ~~(which is significantly larger than the systematic uncertainty estimated for the MUSICA IASI data after its calibration to in-situ aircraft pr~~  
~~. While in the simulations the large majority of the  $\{q, \delta D\}$ -pairs is located above the Rayleigh line, in the observations about half is above and the other half is below the Rayleigh line, i.e. a super-Rayleigh distribution is regularly observed in the real world but very rare in the simulations. Section 6.3 of Diekmann (2021). They are also reported for the isotopologue data~~  
545 ~~Diekmann (2021) documents that the MUSICA IASI  $\{q, \delta D\}$ -pair data observed in the context of the West African Monsoon are generally located below the Rayleigh line if a convective event was happening shortly before the observation, which highlights the strong link between the regularly observed super-Rayleigh distributions and convective processes. This link seems to be weaker in the simulations, i.e. there the convective processes leave a significantly weaker  $\{q, \delta D\}$ -pair signature on the nearby cloud-free atmosphere.~~

#### 4.4 Outlook on assimilating real world $\delta D$ observations

550 ~~Current state-of-the-art satellite sensors allow the observation of  $\delta D$  with high quality and resolution (e.g. Worden et al., 2007; Frankenber~~  
~~. Furthermore,  $\{q, \delta D\}$ -pair super-Rayleigh distributions have been observed in data sets generated from measurements of the TES (Tropospheric Emission Spectrometer) instrument (e.g. in Sect. 4 of Noone, 2012). This demonstrates, that current state-of-the-art infrared satellite instruments like IASI or TES can deliver water vapour isotopologue data for those conditions, under which they are most impacting on the analyses. The satellite instrument (e.g. Noone, 2012) and in the MUSICA IASI data~~  
555 ~~(Schneider et al., 2017; Diekmann et al., 2021a; Diekmann, 2021). As discussed in the previous subsection, these super-Rayleigh distributions contain valuable information on convective processes. In this context, the IASI instrument and thus the MUSICA IASI data set is in particular promising~~  
~~in this context: measurements of IASI (or IASI-NG, the successor instrument of IASI) offer a very high horizontal and spatial coverage, and are guaranteed at least for the next two decades in the framework of the Metop and Metop-SG missions of EUMETSAT (European Organisation for the Exploitation of Meteorological Satel-~~  
560 ~~lites, https://www.eumetsat.int/our-satellites/metop-series), i.e. respective  $\{q, \delta D\}$ -pair observations are guaranteed for the next decades.~~

~~In addition to the availability of observations linked to the most impacting convective conditions~~  
~~However, in order to optimally use these  $\delta D$  observations in data assimilation approaches, we need atmospheric isotopologue enabled models that capture as much as possible details of a convective atmosphere. The here-used model IsoGSM (IsoGSM model used here~~  
565 ~~with  $200 \times 200$  km horizontal resolution ) does generally a good job, which has been demonstrated in different model validation studies (e.g. Yoshimura et al., 2008; Schneider et al., 2010). However, a higher horizontal resolution and a convection permitting model setup (instead of parametrising convection as in IsoGSM ) might further improve the capability of a model for correctly capturing the real-world multi-scale impact of convective events (e.g. Pante and Knippertz, 2019). Fig. 7 reveals that IsoGSM systematically underestimates the impact of convective events on the  $\{q, \delta D\}$ -pair distribution of a cloud-free~~



570 free troposphere, which in turn suggests that in our OSSE study we might underestimate the real remote impact of  $\delta D$  observations on convective events. For achieving the optimal benefit from the real world  $\delta D$  observations via a data assimilation approach, improving the modelled linkage between convective processes and the free tropospheric  $\{q, \delta D\}$ -pair distribution might be an important next step. In this context, the ongoing development of including water isotopologue simulations into different highly resolving models also used for operational weather forecasting (e.g. Pfahl et al., 2012; Eckstein et al., 2018) 575 (e.g. Pfahl et al., 2012; Eckstein et al., 2018; Tanoue et al., 2023) is very encouraging. ~~In future work the LETKF assimilation approach could be used together with a model resolution that comes close to the horizontal resolution of the MUSICA IASI data (10-20 km). Then the model might~~ A higher horizontal resolution and a convection permitting model setup (instead of parametrising convection as in IsoGSM) might further improve the capability of a model for correctly capturing the real world multi-scale impact of convective events (e.g. Pante and Knippertz, 2019) and thus better capture many details of the 580 ~~convective atmosphere and moreover, all MUSICA IASI observations could be used (no averaging/aggregation onto a coarser model grid would be required). On the other hand, using an Ensemble Kalman Filter together with a highly resolving model is computationally very expensive, because the high resolution simulations have to be performed for all the different ensemble members.~~ convective processes (including the simulation of super-Rayleigh distributions).

## 5 Summary

585 We evaluate in detail the quality of the analyses of low latitudinal free tropospheric specific humidity ( $q$ ), temperature ( $T$ ), and water vapour isotopologue ratio ( $\delta D$ ), as well as of the three water cycle variables free tropospheric ~~latent heating rate ( $Q_2$ )~~ vertical velocity ( $\omega$ ), free tropospheric ~~vertical velocity ( $\omega$ )~~ latent heating rate ( $Q_2$ ), and precipitation rate (Prcp). We investigate the impact of assimilating free tropospheric specific humidity and temperature (which can be easily observed by many different techniques) and the possibility of further improving the analyses by additionally assimilating free tropospheric water 590 isotopologue data ( $\delta D$ ), for which nowadays also reliable observations with good horizontal and temporal coverage exist. We assume that the observations are only available for cloud-free conditions.

First, we make a statistical ~~overview~~ overall evaluation considering all locations and time steps. The assimilation of  $q$  and  $T$  observations strongly improves the analyses data quality of  $q$  and  $T$  with skill values of up to 60%, if compared to no data assimilation. Concerning the analyses of the other variables ( $\delta D$ ,  $\omega$ ,  $Q_2$ , and Prcp) we also achieve a strong improvement with 595 skill values of ~~30%-40%~~ 10%-30%. Assimilating  $\delta D$  on top of  $q$  and  $T$  does does strongly further improve the analyses of  $\delta D$  (~~very strongly, with additional skills leading to a skill value of up to 25%~~ 50%). However, ~~the further improvement of the other variables ( $q$ ,  $T$ ,  $\omega$ ,  $Q_2$ , and Prcp) is weak and we found that the overall impact of  $\delta D$  observations on the analyses quality is much smaller than the large impact caused by the observations of  $q$  and Prcp (with additional skills of about 5% and 10%, respectively), and of  $T$  and  $\omega$  (by less than 10% additional skills and an estimated skill uncertainty being slightly larger than 600 ~~the estimated skill value).~~~~

In a second evaluation we investigate how the ~~additional assimilation impact of~~  $\delta D$  observation impact depends on the ~~occurrence of phase transitions (condensation and evaporation leaves unique signatures on  $\delta D$ )~~ atmospheric conditions. We



use atmospheric latent heating ( $Q_2$  vertical velocity ( $\omega$ ) as proxy for phase transitions. The analyses uncertainty of  $\omega$ ,  $Q_2$ , and Prcp is the highest when strong latent heating occurs. We demonstrate that under these conditions the additional assimilation of stable and unstable atmospheric conditions. The large majority of events represent stable conditions, for which the  $\delta D$  observations impact is generally negligible; however, for the rare convective conditions with strongly negative  $\omega$ , the  $\delta D$  on-top of  $q$  and  $T$  has also the largest additional skills (up to 15% for observation impact is significant and for the analyses of the water cycle variables ( $\omega$ ,  $Q_2$ , and Prcp) . Because these strong latent heating events are very rare, the strong impact of the additional  $\delta D$  data assimilation is less clear in an overview evaluation, that considers all events (the large majority of events corresponds to heating rates close to zero, where the addition of  $\delta D$  observations have a very weak impact). However, the rare but strong latent heating events even slightly stronger than the  $T$  observation impact. Although being rare, the very unstable conditions dominate the total yearly-averaged precipitation amounts in many regions and they are also responsible for related to extreme events (e.g. storms, flooding) . Better capturing these events in the analyses has thus a strong that are not well captured in the analyses (for these extreme events also the analyses uncertainties of  $\omega$ ,  $Q_2$ , and Prcp are very large). This means that the  $\delta D$  observations offer potential for better capturing the events with the largest societal impact.

For high heating rates, the additional assimilation of At the location and time of these unstable atmospheric conditions we assimilate no observations in our study. This indicates to a unique remote impact of elsewhere available  $\delta D$  observations can also further improve on the analyses of free-tropospheric  $q$  and  $T$ . This improvement is high in relative metrics (skill values), but small in absolute values, because already the assimilation of  $q$  and  $T$  well constrains the  $q$  and  $T$  analyses. convective events.

The conditions when the additional assimilation of  
A super-Rayleigh  $\{q, \delta D\}$ -pair distribution means high humidity and at the same time strong HDO depletion, and this distribution is linked to convective processes. We think that the conservation of these depleted signals outside of the convecting area (where it can be measured) is essential for the unique remote impact of the  $\delta D$  observations makes an important and unique contribution can be identified in  $\{q, \delta D\}$ -pairs located in the on the analyses of convective processes. In this context, we interpret the regular observation of super-Rayleigh domain. These super-Rayleigh  $\{q, \delta D\}$ -pair distributions are often observed distributions in the MUSICA IASI satellite data. We interpret this data as a promising indication for the possibility of improving the analyses achieving the unique remote impact of  $\delta D$  in the real world similarly to the improvement demonstrated here with our OSSE our OSSE study for a simulated world. Moreover, the A real world  $\delta D$  assimilation works best, if the used model correctly captures the depleted signals of convection. The availability of a growing number of high resolution atmospheric isotopologue enabled models does importantly support importantly supports further progress in this field.

*Data availability.* The nature data and the ensemble mean data of the different assimilation experiments used for this study are available at <https://radar.kit.edu/radar/en/dataset/PJeqXmWILYSGBkJJ?token=rejHyXIETzWLGeopwLNq>. The MUSICA IASI water vapour isotopologue data set is available at <https://doi.org/10.35097/415>.

635 *Author contributions.* Kei Yoshimura developed the isotopologue assimilation framework. Kinya Toride made all the data assimilation experiments. Matthias Schneider developed the ideas for evaluating the analyses improvements achievable by adding  $\delta\text{D}$  observations and made the respective calculations, whereby he was supported by Kinya Toride and Farahnaz Khosrawi. Frank Hase, Benjamin Ertl, and Christopher J. Diekmann provided important contribution for the design of this study. All authors supported the generation of the final version of this manuscript.

640 *Competing interests.* At least one of the (co-)authors is a member of the editorial board of Atmospheric Measurement Techniques.

*Acknowledgements.* This research has benefit from funds of the Deutsche Forschungsgemeinschaft (provided for the project TEDDY, ID 416767181).

Important part of this work was performed on the supercomputer HoreKa funded by the Ministry of Science, Research and the Arts Baden-Württemberg and by the German Federal Ministry of Education and Research.

645 We acknowledge the support by the Deutsche Forschungsgemeinschaft and the Open Access Publishing Fund of the Karlsruhe Institute of Technology.

## References

- Bailey, A., Nusbaumer, J., and Noone, D.: Precipitation efficiency derived from isotope ratios in water vapor distinguishes dynamical and microphysical influences on subtropical atmospheric constituents, *Journal of Geophysical Research: Atmospheres*, 120, 9119–9137, <https://doi.org/https://doi.org/10.1002/2015JD023403>, <https://agupubs.onlinelibrary.wiley.com/doi/abs/10.1002/2015JD023403>, 2015.
- 650 Blossey, P. N., Kuang, Z., and Romps, D. M.: Isotopic composition of water in the tropical tropopause layer in cloud-resolving simulations of an idealized tropical circulation, *Journal of Geophysical Research: Atmospheres*, 115, <https://doi.org/https://doi.org/10.1029/2010JD014554>, <https://agupubs.onlinelibrary.wiley.com/doi/abs/10.1029/2010JD014554>, 2010.
- Boesch, H., Deutscher, N. M., Warneke, T., Byckling, K., Cogan, A. J., Griffith, D. W. T., Notholt, J., Parker, R. J., and Wang, Z.: HDO/H<sub>2</sub>O ratio retrievals from GOSAT, *Atmospheric Measurement Techniques*, 6, 599–612, <https://doi.org/10.5194/amt-6-599-2013>, <http://www.atmos-meas-tech.net/6/599/2013/>, 2013.
- 655 Bony, S., Risi, C., and Vimeux, F.: Influence of convective processes on the isotopic composition ( $\delta^{18}\text{O}$  and  $\delta\text{D}$ ) of precipitation and water vapor in the tropics: 1. Radiative-convective equilibrium and Tropical Ocean–Global Atmosphere–Coupled Ocean–Atmosphere Response Experiment (TOGA-COARE) simulations, *Journal of Geophysical Research: Atmospheres*, 113, <https://doi.org/https://doi.org/10.1029/2008JD009942>, <https://agupubs.onlinelibrary.wiley.com/doi/abs/10.1029/2008JD009942>, 2008.
- 660 Bony, S., Stevens, B., Frierson, D., Jakob, C., Kageyama, M., Pincus, R., Shepherd, T. G., Sherwood, S. C., Siebesma, A. P., Sobel, A. H., Watanabe, M., and Webb, M. J.: Clouds, circulation and climate sensitivity, *Nature Geosci*, 8, 261–268, <https://doi.org/https://doi.org/10.1038/ngeo2398>, 2015.
- Chan, S. C. and Nigam, S.: Residual Diagnosis of Diabatic Heating from ERA-40 and NCEP Reanalyses: Intercomparisons with TRMM, *Journal of Climate*, 22, 414 – 428, <https://doi.org/https://doi.org/10.1175/2008JCLI2417.1>, <https://journals.ametsoc.org/view/journals/clim/22/2/2008jcli2417.1.xml>, 2009.
- 665 Clerbaux, C., Boynard, A., Clarisse, L., George, M., Hadji-Lazaro, J., Herbin, H., Hurtmans, D., Pommier, M., Razavi, A., Turquety, S., Wespes, C., and Coheur, P.-F.: Monitoring of atmospheric composition using the thermal infrared IASI/MetOp sounder, *Atmospheric Chemistry and Physics*, 9, 6041–6054, <https://doi.org/10.5194/acp-9-6041-2009>, <https://acp.copernicus.org/articles/9/6041/2009/>, 2009.
- 670 Craig, H.: Standard for Reporting concentrations of Deuterium and Oxygen-18 in natural waters, *Science*, 13, 1833–1834, <https://doi.org/10.1126/science.133.3467.1833>, 1961.
- Dahinden, F., Aemisegger, F., Wernli, H., Schneider, M., a. D. C. J., Ertl, B., Knippertz, P., Werner, M., and Pfahl, S.: Disentangling different moisture transport pathways over the eastern subtropical North Atlantic using multi-platform isotope observations and high-resolution numerical modelling, *Atmospheric Chemistry and Physics*, 21, 16 319–16 347, <https://doi.org/10.5194/acp-21-16319-2021>, 2021.
- 675 Diekmann, C. J.: Analysis of stable water isotopes in tropospheric moisture during the West African Monsoon, Ph.D. thesis, Karlsruhe Institut für Technologie (KIT), <https://doi.org/10.5445/IR/1000134744>, 2021.
- Diekmann, C. J., Schneider, M., Ertl, B., Hase, F., García, O., Khosrawi, F., Sepúlveda, E., Knippertz, P., and Braesicke, P.: The global and multi-annual MUSICA IASI {H<sub>2</sub>O,  $\delta\text{D}$ } pair dataset, *Earth System Science Data*, 13, 5273–5292, <https://doi.org/10.5194/essd-13-5273-2021>, <https://essd.copernicus.org/articles/13/5273/2021/>, 2021a.
- 680 Diekmann, C. J., Schneider, M., Knippertz, P., de Vries, A. J., Pfahl, S., Aemisegger, F., Dahinden, F., Ertl, B., Khosrawi, F., Wernli, H., and Braesicke, P.: A Lagrangian Perspective on Stable Water Isotopes During the West African Monsoon, *Journal of Geophysical Research: Atmospheres*, 126, e2021JD034 895, <https://doi.org/https://doi.org/10.1029/2021JD034895>, <https://agupubs.onlinelibrary.wiley.com/doi/abs/10.1029/2021JD034895>, e2021JD034895 2021JD034895, 2021b.

- Eckstein, J., Ruhnke, R., Pfahl, S., Christner, E., Diekmann, C., Dyroff, C., Reinert, D., Rieger, D., Schneider, M., Schröter, J., Zahn, A., and Braesicke, P.: From climatological to small-scale applications: simulating water isotopologues with ICON-ART-Iso (version 2.3), *Geoscientific Model Development*, 11, 5113–5133, <https://doi.org/10.5194/gmd-11-5113-2018>, <https://gmd.copernicus.org/articles/11/5113/2018/>, 2018.
- Evans, C., Wood, K. M., Aberson, S. D., Archambault, H. M., Milrad, S. M., Bosart, L. F., Corbosiero, K. L., Davis, C. A., Pinto, J. R. D., Doyle, J., Fogarty, C., Galarneau, T. J., Grams, C. M., Griffin, K. S., Gyakum, J., Hart, R. E., Kitabatake, N., Lentink, H. S., McTaggart-Cowan, R., Perrie, W., Quinting, J. F. D., Reynolds, C. A., Riemer, M., Ritchie, E. A., Sun, Y., and Zhang, F.: The Extratropical Transition of Tropical Cyclones. Part I: Cyclone Evolution and Direct Impacts, *Monthly Weather Review*, 145, 4317 – 4344, <https://doi.org/10.1175/MWR-D-17-0027.1>, <https://journals.ametsoc.org/view/journals/mwre/145/11/mwr-d-17-0027.1.xml>, 2017.
- Eyre, J. R., Bell, W., Cotton, J., English, S. J., Forsythe, M., Healy, S. B., and Pavelin, E. G.: Assimilation of satellite data in numerical weather prediction. Part II: Recent years, *Quarterly Journal of the Royal Meteorological Society*, 148, 521–556, <https://doi.org/https://doi.org/10.1002/qj.4228>, <https://rmets.onlinelibrary.wiley.com/doi/abs/10.1002/qj.4228>, 2022.
- Field, R. D., Jones, D. B. A., and Brown, D. P.: Effects of postcondensation exchange on the isotopic composition of water in the atmosphere, *J. Geophys. Res.*, 115, D24 305, <https://doi.org/10.1029/2010JD014334>, 2010.
- Field, R. D., Kim, D., LeGrande, A. N., Worden, J., Kelley, M., and Schmidt, G. A.: Evaluating climate model performance in the tropics with retrievals of water isotopic composition from Aura TES, *Geophysical Research Letters*, 41, 6030–6036, <https://doi.org/10.1002/2014GL060572>, <http://dx.doi.org/10.1002/2014GL060572>, 2014GL060572, 2014.
- Fink, A. H., Pohle, S., Pinto, J. G., and Knippertz, P.: Diagnosing the influence of diabatic processes on the explosive deepening of extratropical cyclones, *Geophysical Research Letters*, 39, <https://doi.org/10.1029/2012GL051025>, <http://dx.doi.org/10.1029/2012GL051025>, 107803, 2012.
- Frankenberg, C., Yoshimura, K., Warneke, T., Aben, I., Butz, A., Deutscher, N., Griffith, D., Hase, F., Notholt, J., Schneider, M., Schreyver, H., and Röckmann, T.: Dynamic processes governing lower-tropospheric HDO/H<sub>2</sub>O ratios as observed from space and ground, *Science*, 325, 1374–1377, <https://doi.org/10.1126/science.1173791>, 2009.
- Galewsky, J., Steen-Larsen, H. C., Field, R. D., Worden, J., Risi, C., and Schneider, M.: Stable isotopes in atmospheric water vapor and applications to the hydrologic cycle, *Reviews of Geophysics*, 54, 809–865, <https://doi.org/https://doi.org/10.1002/2015RG000512>, <https://agupubs.onlinelibrary.wiley.com/doi/abs/10.1002/2015RG000512>, 2016.
- González, Y., Schneider, M., Dyroff, C., Rodríguez, S., Christner, E., García, O. E., Cuevas, E., Bustos, J. J., Ramos, R., Guirado-Fuentes, C., Barthlott, S., Wiegeler, A., and Sepúlveda, E.: Detecting moisture transport pathways to the subtropical North Atlantic free troposphere using paired H<sub>2</sub>O- $\delta$ D in situ measurements, *Atmospheric Chemistry and Physics*, 16, 4251–4269, <https://doi.org/10.5194/acp-16-4251-2016>, <https://acp.copernicus.org/articles/16/4251/2016/>, 2016.
- Hersbach, H., Bell, B., Berrisford, P., Hirahara, S., Horányi, A., Muñoz Sabater, J., Nicolas, J., Peubey, C., Radu, R., Schepers, D., Simmons, A., Soci, C., Abdalla, S., Abellan, X., Balsamo, G., Bechtold, P., Biavati, G., Bidlot, J., Bonavita, M., De Chiara, G., Dahlgren, P., Dee, D., Diamantakis, M., Dragani, R., Flemming, J., Forbes, R., Fuentes, M., Geer, A., Haimberger, L., Healy, S., Hogan, R. J., Hólm, E., Janisková, M., Keeley, S., Laloyaux, P., Lopez, P., Lupu, C., Radnoti, G., de Rosnay, P., Rozum, I., Vamborg, F., Villaume, S., and Thépaut, J.-N.: The ERA5 global reanalysis, *Quarterly Journal of the Royal Meteorological Society*, 146, 1999–2049, <https://doi.org/https://doi.org/10.1002/qj.3803>, <https://rmets.onlinelibrary.wiley.com/doi/abs/10.1002/qj.3803>, 2020.

- 720 Hunt, B. R., Kostelich, E. J., and Szunyogh, I.: Efficient data assimilation for spatiotemporal chaos: A local ensemble transform Kalman filter, *Physica D: Nonlinear Phenomena*, 230, 112–126, <https://doi.org/https://doi.org/10.1016/j.physd.2006.11.008>, <https://www.sciencedirect.com/science/article/pii/S0167278906004647>, data Assimilation, 2007.
- Kalman, R. E.: A New Approach to Linear Filtering and Prediction Problems, *Journal of Basic Engineering*, 82, 35–45, <https://doi.org/10.1115/1.3662552>, <https://doi.org/10.1115/1.3662552>, 1960.
- 725 Lacour, J.-L., Risi, C., Clarisse, L., Bony, S., Hurtmans, D., Clerbaux, C., and Coheur, P.-F.: Mid-tropospheric  $\delta D$  observations from IASI/MetOp at high spatial and temporal resolution, *Atmospheric Chemistry and Physics*, 12, 10 817–10 832, <https://doi.org/10.5194/acp-12-10817-2012>, <http://www.atmos-chem-phys.net/12/10817/2012/>, 2012.
- Lacour, J.-L., Flamant, C., Risi, C., Clerbaux, C., and Coheur, P.-F.: Importance of the Saharan heat low in controlling the North Atlantic free tropospheric humidity budget deduced from IASI  $\delta D$  observations, *Atmospheric Chemistry and Physics*, 17, 9645–9663, <https://doi.org/10.5194/acp-17-9645-2017>, <https://acp.copernicus.org/articles/17/9645/2017/>, 2017.
- 730 Ling, J. and Zhang, C.: Diabatic Heating Profiles in Recent Global Reanalyses, *Journal of Climate*, 26, 3307 – 3325, <https://doi.org/https://doi.org/10.1175/JCLI-D-12-00384.1>, <https://journals.ametsoc.org/view/journals/clim/26/10/jcli-d-12-00384.1.xml>, 2013.
- Noone, D.: Pairing Measurements of the Water Vapor Isotope Ratio with Humidity to Deduce Atmospheric Moistening and Dehydration in the Tropical Midtroposphere, *J. Climate*, 25, 4476–4494, <https://doi.org/10.1175/JCLI-D-11-00582.1>, 2012.
- 735 Noone, D., Galewsky, J., Sharp, Z. D., Worden, J., Barnes, J., Baer, D., Bailey, A., Brown, D. P., Christensen, L., Crosson, E., Dong, F., Hurley, J. V., Johnson, L. R., Strong, M., Toohey, D., Van Pelt, A., and Wright, J. S.: Properties of air mass mixing and humidity in the subtropics from measurements of the D/H isotope ratio of water vapor at the Mauna Loa Observatory, *Journal of Geophysical Research: Atmospheres*, 116, D22 113, <https://doi.org/https://doi.org/10.1029/2011JD015773>, <https://agupubs.onlinelibrary.wiley.com/doi/abs/10.1029/2011JD015773>, 2011.
- 740 Pante, G. and Knippertz, P.: Resolving Sahelian thunderstorms improves mid-latitude weather forecasts, *Nature Communications*, 10, 3487, <https://doi.org/10.1038/s41467-019-11081-4>, <https://doi.org/10.1038/s41467-019-11081-4>, 2019.
- Pfahl, S., Wernli, H., and Yoshimura, K.: The isotopic composition of precipitation from a winter storm – a case study with the limited-area model COSMO<sub>iso</sub>, *Atmospheric Chemistry and Physics*, 12, 1629–1648, <https://doi.org/10.5194/acp-12-1629-2012>, <https://acp.copernicus.org/articles/12/1629/2012/>, 2012.
- 745 Risi, C., Bony, S., and Vimeux, F.: Influence of convective processes on the isotopic composition ( $\delta^{18}O$  and  $\delta D$ ) of precipitation and water vapor in the tropics: 2. Physical interpretation of the amount effect, *Journal of Geophysical Research: Atmospheres*, 113, <https://doi.org/https://doi.org/10.1029/2008JD009943>, <https://agupubs.onlinelibrary.wiley.com/doi/abs/10.1029/2008JD009943>, 2008.
- Risi, C., Bony, S., Vimeux, F., and Jouzel, J.: Water-stable isotopes in the LMDZ4 general circulation model: Model evaluation for present-day and past climates and applications to climatic interpretations of tropical isotopic records, *Journal of Geophysical Research: Atmospheres*, 115, <https://doi.org/10.1029/2009JD013255>, <https://agupubs.onlinelibrary.wiley.com/doi/abs/10.1029/2009JD013255>, 2010.
- 750 Risi, C., Noone, D., Worden, J., Frankenberg, C., Stiller, G., Kiefer, M., Funke, B., Walker, K., Bernath, P., Schneider, M., Bony, S., Lee, J., Brown, D., and Sturm, C.: Process-evaluation of tropospheric humidity simulated by general circulation models using water vapor isotopic observations. Part 2: an isotopic diagnostic to understand the mid and upper tropospheric moist bias in the tropics and subtropics, *J. Geophys. Res.*, 117, <https://doi.org/10.1029/2011JD016623>, 2012.
- 755 Rodgers, C.: *Inverse Methods for Atmospheric Sounding: Theory and Praxis*, World Scientific Publishing Co., Singapore, 2000.

- Schneider, A., Borsdorff, T., aan de Brugh, J., Aemisegger, F., Feist, D. G., Kivi, R., Hase, F., Schneider, M., and Landgraf, J.: First data set of H<sub>2</sub>O/HDO columns from the Tropospheric Monitoring Instrument (TROPOMI), *Atmospheric Measurement Techniques*, 13, 85–100, <https://doi.org/10.5194/amt-13-85-2020>, <https://amt.copernicus.org/articles/13/85/2020/>, 2020.
- 760 Schneider, M. and Hase, F.: Optimal estimation of tropospheric H<sub>2</sub>O and  $\delta$ D with IASI/METOP, *Atmos. Chem. Phys.*, 11, 11 207–11 220, <https://doi.org/10.5194/acp-11-11207-2011>, 2011.
- Schneider, M., Yoshimura, K., Hase, F., and Blumenstock, T.: The ground-based FTIR network's potential for investigating the atmospheric water cycle, *Atmos. Chem. Phys.*, 10, 3427–3442, <http://www.atmos-chem-phys.net/6/3427/2010/>, 2010.
- Schneider, M., Wiegeler, A., Barthlott, S., González, Y., Christner, E., Dyroff, C., García, O. E., Hase, F., Blumenstock, T., Sepúlveda, E.,  
765 Mengistu Tsidu, G., Takele Kenea, S., Rodríguez, S., and Andrey, J.: Accomplishments of the MUSICA project to provide accurate, long-term, global and high-resolution observations of tropospheric {H<sub>2</sub>O, $\delta$ D} pairs – a review, *Atmospheric Measurement Techniques*, 9, 2845–2875, <https://doi.org/10.5194/amt-9-2845-2016>, <http://www.atmos-meas-tech.net/9/2845/2016/>, 2016.
- Schneider, M., Borger, C., Wiegeler, A., Hase, F., García, O. E., Sepúlveda, E., and Werner, M.: MUSICA MetOp/IASI {H<sub>2</sub>O, $\delta$ D} pair retrieval simulations for validating tropospheric moisture pathways in atmospheric models, *Atmospheric Measurement Techniques*, 10,  
770 507–525, <https://doi.org/10.5194/amt-10-507-2017>, 2017.
- Schneider, M., Ertl, B., Diekmann, C. J., Khosrawi, F., Weber, A., Hase, F., Höpfner, M., García, O. E., Sepúlveda, E., and Kinnison, D.: Design and description of the MUSICA IASI full retrieval product, *Earth System Science Data*, 14, 709–742, <https://doi.org/10.5194/essd-14-709-2022>, <https://essd.copernicus.org/articles/14/709/2022/>, 2022.
- Sherwood, S. C., Bony, S., and Dufresne, J.-L.: Spread in model climate sensitivity traced to atmospheric convective mixing, *Nature*, 505,  
775 37–42, <https://doi.org/10.1038/nature12829>, 2014.
- Tada, M., Yoshimura, K., and Toride, K.: Improving weather forecasting by assimilation of water vapor isotopes, *Scientific Reports*, 11, <https://doi.org/10.1038/s41598-021-97476-0>, 2021.
- Tanoue, M., Yashiro, H., Takano, Y., Yoshimura, K., Kodama, C., and Satoh, M.: Modeling Water Isotopes Using a Global Non-Hydrostatic Model With an Explicit Convection: Comparison With Gridded Data Sets and Site Observations, *Journal of Geophysical Research: Atmospheres*, 128, e2021JD036419, <https://doi.org/https://doi.org/10.1029/2021JD036419>, <https://agupubs.onlinelibrary.wiley.com/doi/abs/10.1029/2021JD036419>, e2021JD036419 2021JD036419, 2023.
- 780 Toride, K., Yoshimura, K., Tada, M., Diekmann, C., Ertl, B., Khosrawi, F., and Schneider, M.: Potential of Mid-tropospheric Water Vapor Isotopes to Improve Large-Scale Circulation and Weather Predictability, *Geophysical Research Letters*, 48, e2020GL091698, <https://doi.org/10.1029/2020GL091698>, <https://agupubs.onlinelibrary.wiley.com/doi/abs/10.1029/2020GL091698>, 2021.
- 785 Webster, C. R. and Heymsfield, A. J.: Water Isotope Ratios H/D, <sup>18</sup>O/<sup>16</sup>O, <sup>17</sup>O/<sup>16</sup>O in and out of Clouds Map Dehydration Pathways, *Science*, 302, 1742–1745, <https://doi.org/10.1126/science.1089496>, 2003.
- Werner, M., Langebroek, P. M., Carlsen, T., Herold, M., and Lohmann, G.: Stable water isotopes in the ECHAM5 general circulation model: Toward high-resolution isotope modeling on a global scale, *Journal of Geophysical Research: Atmospheres*, 116, <https://doi.org/https://doi.org/10.1029/2011JD015681>, <https://agupubs.onlinelibrary.wiley.com/doi/abs/10.1029/2011JD015681>, 2011.
- 790 Wilks, D. S.: *Statistical methods in the atmospheric sciences*, Elsevier, <https://doi.org/10.1016/C2017-0-03921-6>, 2019.
- Worden, J., Noone, D., Bowman, K., Beer, R., Eldering, A., Fisher, B., Gunson, M., Goldman, A., Herman, R., Kulawik, S. S., Lampel, M., Osterman, G., Rinsland, C., Rodgers, C., Sander, S., Shephard, M., Webster, R., and Worden, H.: Importance of rain evaporation and continental convection in the tropical water cycle, *Nature*, 445, 528–532, <https://doi.org/10.1038/nature05508>, 2007.

- Worden, J. R., Kulawik, S. S., Fu, D., Payne, V. H., Lipton, A. E., Polonsky, I., He, Y., Cady-Pereira, K., Moncet, J.-L., Herman, R. L., Irion, F. W., and Bowman, K. W.: Characterization and evaluation of AIRS-based estimates of the deuterium content of water vapor, *Atmospheric Measurement Techniques*, 12, 2331–2339, <https://doi.org/10.5194/amt-12-2331-2019>, <https://amt.copernicus.org/articles/12/2331/2019/>, 2019.
- 795
- Yanai, M., Esbensen, S., and Chu, J.-H.: Determination of Bulk Properties of Tropical Cloud Clusters from Large-Scale Heat and Moisture Budgets, *Journal of Atmospheric Sciences*, 30, 611 – 627, [https://doi.org/10.1175/1520-0469\(1973\)030<0611:DOBPOT>2.0.CO;2](https://doi.org/10.1175/1520-0469(1973)030<0611:DOBPOT>2.0.CO;2), [https://journals.ametsoc.org/view/journals/atsc/30/4/1520-0469\\_1973\\_030\\_0611\\_dobpot\\_2\\_0\\_co\\_2.xml](https://journals.ametsoc.org/view/journals/atsc/30/4/1520-0469_1973_030_0611_dobpot_2_0_co_2.xml), 1973.
- 800
- Yoshimura, K., Kanamitsu, M., Noone, D., and Oki, T.: Historical isotope simulation using Reanalysis atmospheric data, *J. Geophys. Res.*, 113, D19 108, <https://doi.org/10.1029/2008JD010074>, 2008.
- Yoshimura, K., Miyoshi, T., and Kanamitsu, M.: Observation system simulation experiments using water vapor isotope information, *Journal of Geophysical Research: Atmospheres*, 119, 7842–7862, <https://doi.org/https://doi.org/10.1002/2014JD021662>, <https://agupubs.onlinelibrary.wiley.com/doi/abs/10.1002/2014JD021662>, 2014.
- 805